2015

Geochemistry and age of mafic rocks from the Votuverava Group, southern Ribeira Belt, Brazil: evidence for 1490Ma oceanic back-arc magmatism

G A. C Campanha
Cidade Universitaria

F M. Faleiros
Cidade Universitaria

Miguel Angelo Stipp Basei
Cidade Universitaria, baseimas@usp.br

C C. G Tassinari
Cidade Universitaria

Allen Phillip Nutman
University of Wollongong, anutman@uow.edu.au

See next page for additional authors

Publication Details

Campanha, G. A. C., Faleiros, F. M., Basei, M. A. S., Tassinari, C. C. G., Nutman, A. P. & Vasconcelos, P. M. (2015). Geochemistry and age of mafic rocks from the Votuverava Group, southern Ribeira Belt, Brazil: evidence for 1490Ma oceanic back-arc magmatism. Precambrian Research, 266 530-550.

Geochemistry and age of mafic rocks from the Votuverava Group, southern Ribeira Belt, Brazil: evidence for 1490Ma oceanic back-arc magmatism

Abstract

This paper presents new SHRIMP U-Pb zircon and 40Ar-39Ar hornblende ages as well as elemental and Sr-Nd isotopic data for greenschist to amphibolite facies meta-mafic rocks from the Votuverava Group (Ribeira Belt, Brazil). These mafic rocks appear to be mostly subvolcanic and volcanic rocks and, in part, intrusions coeval with the host sedimentary succession. Magmatic zircons have a U-Pb age of 1488 ± 4 Ma. An 40Ar-39Ar hornblende age of 1390 ± 20 Ma suggests cooling after a thermal event. The mafic rocks have chemical compositions of basalt and basaltic andesite (SiO_2 of 45-55 wt.%) of the tholeiitic series. Chemical data indicate the coexistence of rocks with BABB and E-MORB signatures. BABB-like rocks with a Ti/V of 9-20 show depletion in HFSE relative to MORB values and slightly fractionated REE patterns (Lacn/Ybcn of 0.8-1.8), while those with a Ti/V of 22-30 have HFSE contents similar to MORB and slightly more fractionated REE patterns (Lacn/Ybcn of 1.1-2.8). E-MORB-like rocks display a Ti/V of 27-41 and moderately fractionated REE patterns (Lacn/Ybcn of 3.6-5.3). The $\varepsilon Nd(t)$ values ranged from −3.02 to +3.55. Whole rock Sm-Nd isotopic data yielded a regression with a slope of 1225 ± 68 Ma, which can be interpreted as a mixing line of no age significance that is related to different source components of the metabasic rocks. Elemental and Nd isotopic signatures suggest that the Votuverava metabasites originated from a MORB-type mantle source heterogeneously metasomatized by subduction processes. The data are consistent with magmatic activity in a back-arc basin environment. The 1490 Ma mafic magmatism is associated with a 500-km-long and 60-km-wide Calymmian belt interpreted as an accretionary orogen. Available thermochronological data suggest that this accretionary orogen could have evolved into a collisional orogen in the period 1280-1100 Ma, possibly related to the assembly of Rodinia. During the Brasiliano-Pan African cycle (650-550 Ma), related to amalgamation of West Gondwana, this Calymmian belt represented by the Votuverava Group was dispersed as an exotic terrane along the Ribeira Belt.

Disciplines

Medicine and Health Sciences | Social and Behavioral Sciences

Publication Details

Campanha, G. A. C., Faleiros, F. M., Basei, M. A. S., Tassinari, C. C. G., Nutman, A. P. & Vasconcelos, P. M. (2015). Geochemistry and age of mafic rocks from the Votuverava Group, southern Ribeira Belt, Brazil: evidence for 1490Ma oceanic back-arc magmatism. Precambrian Research, 266 530-550.

Authors

G A. C Campanha, F M. Faleiros, Miguel Angelo Stipp Basei, C C. G Tassinari, Allen Phillip Nutman, and Paulo Vasconcelos

Geochemistry and age of mafic rocks from the Votuverava Group, southern Ribeira Belt, Brazil: evidence for 1490 Ma oceanic back-arc magmatism

Campanha, G.A.C.[1], Faleiros, F.M.[1*], Basei, M.A.S.[1], Tassinari, C.C.G.[1], Nutman, A.P.[2,3,4], Vasconcelos, P.M.[5]

Published in: Precambrian Research, v. 266, p. 530-550.

[1] Instituto de Geociências da Universidade de São Paulo, Rua do Lago, 562, Cidade Universitária, CEP 05508-080, São Paulo, SP, Brazil

[2] GeoQuEST Research Centre, School of Earth & Environmental Sciences, University of Wollongong, Wollongong, NSW 2522, Australia

[3] Beijing SHRIMP Center, Institute of Geology, Chinese Academy of Geological Sciences, Beijing, Peoples Republic of China

[4] Research School of Earth Sciences, Australian National University, Canberra, ACT 0200, Australia

[5] Department of Earth Sciences, University of Queensland, Brisbane, Qld 4072, Australia

*Corresponding author: fax: +55 11 3091 4258, e-mail: ffalei@usp.br

Abstract

This paper presents new SHRIMP U–Pb zircon and ^{40}Ar–^{39}Ar hornblende ages as well as elemental and Sr-Nd isotopic data for greenschist to amphibolite facies meta-mafic rocks from the Votuverava Group (Ribeira Belt, Brazil). These mafic rocks appear to be mostly subvolcanic and volcanic rocks and, in part, intrusions coeval with the host sedimentary succession. Magmatic zircons have a U–Pb age of 1488 ± 4 Ma. An ^{40}Ar–^{39}Ar hornblende age of 1390 ± 20 Ma suggests cooling after a thermal event. The mafic rocks have chemical compositions of basalt and basaltic andesite (SiO_2 of 45-55 wt. %) of the tholeiitic series. Chemical data indicate the coexistence of rocks with BABB and E-MORB signatures. BABB-like rocks with a Ti/V of 9-20 show depletion in HFSE relative to MORB values and slightly fractionated REE patterns (La_{cn}/Yb_{cn} of 0.8-1.8), while those with a Ti/V of 22-30 have HFSE contents similar to MORB and slightly more fractionated REE patterns (La_{cn}/Yb_{cn} of 1.1-2.8). E-MORB-like rocks display a Ti/V of 27-41 and moderately fractionated REE patterns (La_{cn}/Yb_{cn} of 3.6-5.3). The $\varepsilon_{Nd}(t)$ values ranged from -3.02 to +3.55. Whole rock Sm–Nd isotopic data yielded a regression with a slope of 1225 ± 68 Ma, which can be interpreted as a mixing line of no age significance that is related to different source components of the metabasic rocks. Elemental and Nd isotopic signatures suggest that the Votuverava metabasites originated from a MORB-type mantle source heterogeneously metasomatized by subduction processes. The data are consistent with magmatic activity in a back-arc basin environment. The 1490 Ma mafic magmatism is associated with a 500-km-long and 60-km-wide Calymmian belt interpreted as an accretionary orogen. Available thermochronological data suggest that this accretionary orogen could have evolved into a collisional orogen in the period 1280-1100 Ma, possibly related to the

assembly of Rodinia. During the Brasiliano-Pan African cycle (650-550 Ma), related to amalgamation of West Gondwana, this Calymmian belt represented by the Votuverava Group was dispersed as an exotic terrane along the Ribeira Belt.

Keywords: Ribeira belt; Votuverava Group Calymmian magmatism; basic magmatism; back-arc basin; geochronology

1. Introduction

The Ribeira Belt is a Neoproterozoic (Brasiliano–Pan African) accretionary-to-collisional orogen parallel to the southeastern Brazilian coast whose development was related to the assembly of West Gondwana. Neoproterozoic ages for extensive arc-related granitic plutonism and collisional metamorphism are well documented in the orogen (Janasi et al., 2001; Passarelli et al., 2004; Prazeres Filho, 2005; Silva et al., 2005; Cury, 2009; Faleiros et al., 2010, 2011a; Salazar et al., 2013). However, the depositional ages of the majority of supracrustal rock successions, as well as of the related magmatism, are still uncertain and are debated due to the scarcity of robust geochronological data. Historically, the metasedimentary rock units of the southern Ribeira Belt have been inferred to be of Neoproterozoic age and are sometimes considered sedimentation associated with a Neoproterozoic suprasubduction zone environment (Soares, 1987; Fiori, 1992; Reis Neto, 1994; Campanha and Sadowski, 1999; Siga Jr. et al., 2009). Alternatively, Mesoproterozoic ages have been proposed, with continental rift, passive margin continental platform, back-arc basin, fore-arc basin or intra-arc settings (Campanha and Sadowski, 1999; Siga Jr. et al., 2009, 2010, 2011; Faleiros et al., 2011b). Recent geochronological data have demonstrated the existence of imbricated Calymmian, Tonian, Cryogenian and Ediacaran metasedimentary rock units (Hackspacher et al., 2000; Campanha et al., 2008; Cury, 2009; Siga Jr. et al., 2009, 2011a,b), thereby demonstrating a complex crustal architecture. An important remaining question is which supracrustal units formed in the Mesoproterozoic and Neoproterozoic, and what were their tectonic environments? This has significant implications for the understanding of the tectonic process involved in the assembly of West Gondwana and possibly on the configuration of older Proterozoic supercontinents. The existence of

Calymmian-age units raises the possibility of an evolutionary history linked in part with the evolution of the Mesoproterozoic supercontinent Columbia (Rogers and Santosh, 2002; Roberts, 2012, 2013).

The southern Ribeira Belt is divided into the Apiaí and Curitiba terranes, separated by the Lancinha–Cubatão fault zone (Faleiros et al., 2011a). The Votuverava Group is a major metavolcano-sedimentary unit of the Apiaí Terrane (Fig. 1), which is composed of distal turbidites with significant basic magmatism represented by concordant lenses of (metamorphosed) mafic rocks. Previous geochronological studies performed on mafic rocks from restricted portions of the Votuverava Group have provided conflicting results, indicating either Ediacaran (Hackspacher et al., 2000) or Calymmian (Siga Jr. et al., 2011a) ages. The tectonic setting of the basic magmatism is also debated. Some authors consider it as reflecting extensional events related to the break-up of continental masses and the development of large peri-oceanic sedimentary basins (Siga Jr. et al., 2011a,b), whereas other authors interpret this magmatism as associated with back-arc basin environments (Hackspacher et al., 2000; Faleiros et al., 2011b).

This contribution examines metabasic rocks from the Votuverava Group through geochronological analyses (zircon U–Pb by SHRIMP, hornblende ^{40}Ar–^{39}Ar), isotopic geochemistry (whole-rock Sm–Nd and Rb–Sr) and major and trace element geochemistry. This study has three objectives: (1) to recognize the tectonic setting of the basic magmatism, (2) to establish the age of the basic magmatic event and thereby constrain when the host sedimentary succession was deposited and (3) to detect any record of tectonic events prior to the Neoproterozoic Brasiliano-Pan African cycle. The results from this work contribute to the elucidation of the tectonic evolution of the

southern Ribeira Belt and West Gondwana. Possible links with the evolutionary histories of the Proterozoic supercontinents Columbia and Rodinia are also discussed.

2. Geological setting

The Ribeira Belt is a large crustal domain parallel to the coastline of southeastern Brazil, whose components were amalgamated, deformed and metamorphosed during the Brasiliano/Pan African orogeny (Neoproterozoic to beginning of the Paleozoic) related to the assembly of West Gondwana. It has counterparts in the Kaoko and West Congo Belts in western Africa (Almeida et al., 1973). The southern Ribeira Belt evolved from a ca. 650-600 Ma accretionary orogen with extensive arc-related granitic magmatism (Janasi et al., 2001; Prazeres Filho, 2005; Silva et al., 2005) to a ca. 600-590 Ma collisional orogen with associated granitic magmatism (Prazeres Filho et al., 2005; Silva et al., 2005) and associated metamorphism (Faleiros et al., 2010, 2011a). The main cratonic masses involved in this collisional process are the São Francisco-Congo, Paranapanema, Luís Alves and Rio de la Plata cratons (Fig. 1a). The main structures in the Ribeira Belt are controlled by a orogen-parallel continental-scale dextral strike-slip shear system (e.g., Sadowski, 1991; Dürr and Dingeldey, 1996; Campanha, 2002; Egydio-Silva et al., 2002; Campanha e Brito Neves, 2004; Faleiros et al., 2007, 2010, 2011a). As a result, the belt is dominated by tectono-stratigraphic terranes (in the sense of Howell, 1995) of distinct origins, separated by shear zones (Heilbron et al. 2004; Campanha and Faleiros, 2005; Faleiros, 2008; Faleiros et al., 2011a).

The southern Ribeira Belt is divided into the Apiaí and Curitiba composite terranes, separated by the Lancinha–Cubatão fault zone (Fig. 1b). The Curitiba Terrane is composed of migmatitic orthogneisses of the Atuba Complex (Archaean to

Paleoproterozoic) and metamorphosed passive margin continental platform successions of the Turvo-Cajati and Capirú Formations. The Atuba Complex underwent two main episodes of high-grade metamorphism at 2100-2000 Ma and 650-550 Ma, indicating that it represents a fragment of a Rhyacian-Orosirian mobile belt that was intensely reworked in the Brasiliano collisional orogen (Siga Jr., 1995; Sato et al., 2003, 2009; Faleiros et al., 2011a). The Capirú and Turvo-Cajati Formations underwent high-pressure metamorphism, with maximum conditions of 800-820°C, 10-12 kbar and clockwise P-T-t (pressure-temperature-time) paths recorded in the Turvo-Cajati Formation (Faleiros et al., 2011a). Monazite U-Th-Pb chemical dating by electron microprobe yields an age of 589 ± 12 Ma for the peak metamorphism (Faleiros et al., 2011a).

Available U-Pb mineral isotopic data (Hackspacher et al., 2000; Weber et al., 2004; Campanha et al., 2008, 2009; Siga Jr. et al., 2009, 2011a,b) indicate that the Apiaí Terrane was formed by the amalgamation of supracrustal rock units whose ages ranged from Calymmian (ca. 1500-1400 Ma: Água Clara and Betara Formations and Votuverava Group), to Stenian to Tonian (1200-880 Ma: Lajeado Group), to Tonian (1000-900 Ma: part of the Itaiacoca Group) and to Ediacaran (630-580 Ma: part of the Itaiacoca Group and the Iporanga Formation). The supracrustal rock units of the Apiaí Terrane underwent a Barrovian-type clockwise P-T-t loop metamorphism (Faleiros, 2003, 2008; Faleiros et al., 2010) that, according to K–Ar and Rb–Sr isotopic data, has been inferred to be of Neoproterozoic age (Campanha and Sadowski, 1999). Nevertheless, robust dating of accessory metamorphic minerals has not been performed until now. Paleoproterozoic basement rocks occur in restricted nuclei, such as the Tigre Gneiss, which is composed of heterogeneously sheared syenogranite with a chemical signature of extensional A-Type granites and with zircon U–Pb ages of 1772 ± 10 Ma

and 1748 ± 5 Ma (Cury et al., 2002). The Curitiba and Apiaí terranes were intruded by Neoproterozoic granitic plutons (ca. 650-580 Ma) formed in accretionary, collisional and post-collisional episodes (Janasi et al., 2001; Prazeres Filho, 2005; Silva et al., 2005).

2.1. The Votuverava Group

The Votuverava Group was originally defined as a formation in Brazil's Paraná State (Bigarella and Salamuni, 1958) and later extended to São Paulo State (MMAJ/JICA, 1981, 1982, 1983; Chiodi Filho, 1984; Stein et al., 1986; Campanha et al., 1986; Campanha, 1991; Campanha and Sadowski, 1999). In its current usage, the Votuverava Group (e.g., Faleiros et al., 2010, 2012, Faleiros and Pavan, 2013) includes the Perau, Rubuquara, Nhunguara, Piririca and Ribeirão das Pedras Formations (Piekarz, 1981; Takahashi *et al*. 1981; Campos Neto, 1983; Perrota, 1996) and other informal or undivided units (Fig. 2). However, it excludes the major carbonate shelf sequences, such as the Lajeado and Antinha groups (Campanha and Sadowski, 1999) and the Ediacaran Iporanga Formation (Leonardos, 1934, Campanha et al., 2008).

The Votuverava Group is composed of metamorphosed fine-grained pelitic successions (slate, phyllite and schist), generally interpreted as distal turbidites. A large number of metabasites and metavolcanic intercalations also occur, together with local and subordinate occurrences of quartzite, calc-silicate rocks, marble and oligomictic metaconglomerate, the last interpreted as channelized dense turbidite flows. Some paleoenvironmental indicators have been found, such as graded bedding in turbidites. There are also thin layers of iron formations, metachert and minor Pb-Zn-Ag-Cu sulfide deposits (Campanha, 1991; Daitx, 1996).

The dominant deformation style of the Votuverava Group is isoclinal folding, with a NE-trending, steep axial planar slatey cleavage or schistosity usually dipping toward the NW. This foliation is locally cut by a near-vertical crenulation cleavage. Kinks and chevrons with vertical NW-striking axial planes and steeply plunging hinges may be sporadically observed cutting the isoclinal structures. There are rare broad and open late antiforms and synforms developed on a bedding-parallel schistosity. A late system of ductile transcurrent shear zones gives rise to the regional configuration of mega shear lenses.

The rocks of the Votuverava Group display a Barrovian-type metamorphic facies series (Miyashiro, 1961, 1973) ranging from lower greenschist (chlorite zone) north of the Ribeira Shear Zone to medium amphibolite facies conditions (kyanite zone) south of this structure (Faleiros, 2003, 2008; Faleiros and Campanha, 2004; Faleiros et al., 2010). Geothermobarometric data obtained from metapelitic and metabasic rocks from the chlorite to the garnet zone yield peak metamorphic conditions of 380 to 630°C and 6-8 kbar as well as clockwise P-T-t paths (Faleiros et al., 2010).

Available geochemical analyses of metabasic rocks (Campanha, 1991; Frascá et al., 1997; Faleiros et al., 2011b) indicate chemical signatures of both mid-ocean ridge basalts (MORB) and immature island arc basalts.

An Rb–Sr reference isochron from the Perau Formation yielded a 1212 + 55 Ma age with an initial ratio of 0.711 (Batolla Jr. et al.,1981, Teixeira, 1982). Pb–Pb determinations on galenas from the Perau Formation indicate mantle model ages of approximately 1700 Ma (Tassinari *et al*., 1990). Nogueira (1990) obtained Pb-Pb model ages of 1270 Ma and 1303 Ma for galena crystals that occur in Au mineralizations of the Piririca Formation. An Rb–Sr isochron of high-K metavolcanic rocks in the Perau Formation yield an age of 1283 ± 28 Ma (Daitx, 1996). Rb–Sr isochron ages of

approximately 700 and 750 Ma with large uncertainties in slates, phyllites and pelitic schists have been interpreted as being due to the metamorphism related to the Brasiliano-Pan African cycle (Campanha, 1991; Daitx, 1996). Zircon U-Pb ages obtained from metabasites of a restricted area south of the present study (Fig. 2) provided Calymmian ages for the Perau Formation: 1484 ± 16 Ma (SHRIMP), 1479 ± 12 Ma and 1451 ± 39 Ma (ID-TIMS) (Siga Jr. et al., 2011a).

2.2. Field setting and petrography of the Votuverava meta-mafic rocks

The Votuverava metabasites occur exclusively as concordant lenticular bodies with widths ranging from one meter to one kilometer. In most localities, the superimposed high strain during regional metamorphism has obliterated the relationships of the metabasites with adjacent sedimentary rocks. Furthermore, because of the competent nature of the metabasites relative to the surrounding rocks, they now largely occur as lenticular bodies. Locally, however, in rare low strain zones, it is observed that the rocks preserve igneous textures, essentially of very fine- to fine-grained size, suggesting that the metabasites are of a volcanic to subvolcanic nature, probably coeval with the host sedimentary succession.

Two main types of metabasites occur: fine-grained, with an isotropic or slatey structure and a pale green color, and a medium- to coarse-grained variety with a dark green color and a lens-like structure (often mylonitic). The former occurs mainly north of the Ribeira Shear Zone and the second south of it. These two rock types correspond to associations of contrasting metamorphic grades. The first association has actinolite + chlorite + epidote ± plagioclase ± quartz ± carbonate (greenschist facies), and the other has hornblende (tschermakite) + plagioclase (andesine) + quartz ± actinolite ± epidote

(epidote-amphibolite and amphibolite facies). Common accessory minerals include titanite, titanium oxides (Ti-magnetite, ilmenite and rutile) and apatite.

The amphibolite facies metabasites exhibit a nematoblastic texture formed by prismatic amphibole with a preferred orientation. Plagioclase and quartz usually form bands with a granoblastic texture alternated with amphibole-rich bands. One- to two-millimeter porphyroblasts of hornblende, plagioclase and opaque minerals stand out in some samples. The porphyroblasts of amphibole present in the amphibolite facies metabasites generally exhibit textural and chemical zoning related to the progression of metamorphism with actinolitic cores and tschermakitic rims (Faleiros et al., 2010).

Isotropic textures predominate in the greenschist facies metabasites. Locally, subophitic and intergranular igneous textures and remnants of relict igneous clinopyroxene and hornblende are preserved. The igneous hornblende has a dark brown color and is in disequilibrium with the surrounding metamorphic mineral associations. It is petrographically very distinct from the metamorphic hornblende of the amphibolite facies metabasites, which features a dark bluish green color. Mineral chemical analyses performed in dark brown amphibole revealed a composition ranging from edenite to pargasite and ferrous pargasite, corroborating its igneous nature (Maniesi, 1997). These relict igneous textures and minerals indicate that at least some of the metabasite protoliths crystallized from hydrous magmas.

3. Analytical methods

Major and trace elements, including rare earth elements (REEs), of 22 metabasic samples (Table 1) were determined at Activation Laboratories Ltd. (Actlabs, Canada). Major and minor oxides were determined by inductively coupled plasma optical

emission spectrometry (ICP-OES) and trace elements by inductively coupled plasma mass spectrometry (ICP-MS). These new data were integrated with available chemical data (Faleiros et al., 2011b; Table 2) obtained using the same methods at Acme Analytical Laboratories Ltd. (Canada), giving a total of 42 analyses. Some of the geochemical diagrams were produced using the GCDkit program (Janousek et al., 2006; 2011).

Zircons were extracted from 100-200-mesh fractions using standard isodynamic and gravimetric techniques at the Geochronology Research Center of the University of São Paulo (CPGeo-USP). The zircons were hand-picked using a binocular microscope and mounted in epoxy together with grains of the FC1 U-Pb calibration standard and then polished to reveal cross sections through the grains. Cathodoluminescence (CL) and scanning electron microscope (SEM) images were used to identify the best domains for U-Pb analysis, avoiding fractures, inclusions or metamict areas that may have experienced Pb loss. Sensitive high-resolution ion microprobe (SHRIMP) U-Pb analyses were performed using a ~25-µm-diameter spot at the Australian National University. Details of the analytical procedure, as well as of the calculation of the analytical errors, are presented in Stern (1998) and Williams (1998). The decay constants and current $^{238}U/^{235}U$ of Steiger & Jager (1977) were used to calculate ages. U concentrations were calculated using the SL13 standard (U=238 ppm), and $^{206}Pb/^{238}U$ ratios were calibrated using the FC1 standard (concordant, 1099 Ma; Paces and Miller, 1993). The data were presented graphically, and ages were calculated using the Isoplot program (Ludwig, 2003). Data were corrected for common Pb based on measured ^{204}Pb and the Cumming and Richards (1975) model Pb composition for the likely age of the zircons.

^{40}Ar-^{39}Ar analyses were performed in relict igneous hornblende grains extracted from a greenschist facies metabasic rock sample (GD-456) from the Nhunguara Formation of the Votuverava Group at the University of Queensland Argon Geochronology Earth Sciences Laboratory. Hornblende grains 0.5-2 mm in size were placed in aluminum irradiation disks along with Fish Canyon sanidine standards (28.02 ± 0.28 Ma; Renne et al., 1998). Two aliquots were analyzed by laser incremental ^{40}Ar–^{39}Ar step heating following the procedures detailed in Vasconcelos et al. (2002). The main objective of this study is to evaluate whether the igneous hornblende grains were affected by an Ediacaran metamorphic event or if they record distinct cooling ages related to pre-Ediacaran igneous crystallization or metamorphism.

Whole rock Rb–Sr and Sm–Nd isotopic analyses were performed on 14 samples of metabasic rocks using a VG-354 multi-collector mass-spectrometer at the CPGeo-USP, with analytical procedures described in Torquato and Kawashita (1994) and Sato et al. (1995), respectively. The mass fractionation corrections for the Sr and Nd isotopic ratios are based on ^{86}Sr/^{88}Sr=0.1194 and ^{146}Nd/^{144}Nd=0.7219, respectively. The total procedure blanks were within the range of 0.003 µg for Sr, 100-300 pg for Sm and ~50 pg for Nd. The analytical reproducibility was controlled using the NBS-987 standard for the Rb–Sr method and the La Jolla and BCR-1 standards for the Sm–Nd method.

4. Results

4.1. Whole rock geochemistry

Forty-two whole rock geochemical analyses of metabasic rocks are presented in Tables 1 and 2. The analyzed mafic rocks can be divided in three groups based on the

Ti/V versus Nb/Yb ratios (Fig. 3a), which mostly vary within the ranges of 9-21 and 0.7-2.4 (B1), 22-30 and 1.8-3.3 (B2) and 27-41 and 4.9-7.0 (B3), respectively. Petrographically, B1 and B2 are enriched in titanite, plagioclase and quartz and depleted in titanomagnetite and ilmenite in relation to the B3. There is no correlation among the chemical groups, the host rock formations or the variation in the metamorphic grade.

The SiO_2 content varies from 45 to 54 wt. % (anhydrous basis), indicating an essentially basic composition, with all samples exhibiting normative quartz. There is a progressive increase in the Fe_2O_3, TiO_2 and P_2O_5 and a decrease in the MgO and CaO from B1 to B3 (Tables 1 and 2). The rocks display essentially tholeiitic signatures, as seen in AFM and TAS diagrams (Fig. 3b,c), with only three samples classified as basaltic andesite. There is an incremental increase in the contents of the high field strength elements (HFSE) (e.g., Zr, Y, Hf, Nb, Nd, Ta) from B1 to B3 (Tables 1 and 2; Fig. 3d). Additionally, some B3 rocks display anomalously high HFSE contents (e.g., Y, Nb and Zr; Fig. 3d, Tables 1 and 2). The sub-alkaline basaltic signature of the rocks is highlighted in the Winchester and Floyd (1977) diagram, which uses the Zr/TiO_2 ratio as an index of differentiation and the Nb/Y ratio as a discriminant of alkalinity (Fig. 3e). This shows a progressive increase in the alkalinity from B1 to B3.

The three groups B1-B3 exhibit distinct chondrite-normalized (cn) REE patterns and MORB-normalized (mn) patterns. B1 rocks show an REE concentration of three to 13 times the chondrite values, slightly fractionated patterns with an $(La/Yb)_{cn}$ ratio from 0.8 to 1.8 and weak negative anomalies of Ce and positive anomalies of Eu (Fig. 4a-d). In the MORB-normalized diagram (Fig. 4e-h), the B1 samples show strong to weak depletion in HFSEs (from Nd to Yb), with an $(Nb/Yb)_{mn}$ ratio from 0.9 to 3.1 (average value of 1.9). A weak to strong Nb-Ta negative anomaly is present in the majority of the samples (Fig. 4e-h), with Nb/Nb* values (= $Nb_{mn}/[(Th_{mn}+La_{mn})/2]$, normalizing values

of the N-MORB of Sun and McDonough, 1989) from 0.2 to 1.1 (average of 0.6). There is a general enrichment in large ion lithophile elements (LILEs), with Rb, Ba and Th contents up to 30, 20 and seven times the MORB values, respectively. Most samples present strong positive anomalies of K, Pb and Sr (Fig. 4e), but there is no consistency in the behavior of the LILEs, and some samples present weak to strong negative anomalies of K and/or Pb and/or Sr (Fig. 4f-h).

The B2 rocks show an REE concentration from eight to 35 times that of chondrite, slightly fractionated patterns, with an $(La/Yb)_{cn}$ ratio from 1.1 to 2.8 and weak positive anomalies of Nd (Fig. 5a-c). In the MORB-normalized diagrams (Fig. 5d-f), the B2 samples display HFSE contents (from Zr to Yb) approximate to the MORB values with progressive enrichment toward the most incompatible elements, with an $(Nb/Yb)_{mn}$ ratio ranging from 1.8 to 4.4 (average value of 3.2). There is a general enrichment in LILEs, and the Th values reach up to seven times the MORB values. Nevertheless, the behavior of most LILEs, particularly K, Pb and Sr, is inconsistent, displaying strong positive to strong negative anomalies (Fig. 5d-f). A negative Nb-Ta anomaly is present in most samples, particularly those with the lowest Ti/V ratios (e.g., 501, Fig. 5e), and the Nb/Nb* ratio varies from 0.4 to 1.0.

The B3 samples show higher REE concentrations in relation to the other groups, with up to 60 times the chondrite values, moderately fractionated patterns with an $(La/Yb)_{cn}$ ratio from 3.6 to 5.3, and a slightly positive anomaly of Nd (Fig. 6a-c). MORB-normalized patterns are characterized by progressive enrichment in HFSEs toward the most incompatible elements, with $(Nb/Yb)_{mn}$ ratios from 6.5 to 9.2; Y, Ho and Er contents similar to the MORB values; and weak depletion in Yb (Fig. 6d-f). There is a general relative enrichment in LILEs, with all samples displaying a negative K anomaly and most samples exhibiting a positive Sr anomaly (Fig. 6d-f). The

behaviors of Ba and Pb are inconsistent, presenting positive or negative anomalies (Fig. 6d-f). A weak Nb negative anomaly is present in all samples (Nb/Nb* ratios between 0.5 and 0.7).

4.2. U–Pb SHRIMP geochronology

Sample GI-7C is a light green mafic granofels of the Rubuquara Formation that is composed essentially of epidote, actinolite and chlorite. Plagioclase, sericite, titanite, quartz and apatite are the main accessory phases. The rock is fine- to medium-grained, isotropic and presents a preserved subophitic igneous texture with tabular relicts of plagioclase almost completely replaced by cryptocrystalline aggregates of epidote + chlorite ± sericite, along with pseudomorphs of mafic igneous minerals replaced by intergrowths of actinolite and chlorite.

Sample GI-7C yielded 100-200-µm anhedral to subhedral zircon grains with aspect ratios of 1.5:1 to 5:1 (Fig. 7). In the CL images, some grains appear dark and structureless, whereas others are brighter and have igneous oscillatory compositional zoning (Fig. 5). Fourteen SHRIMP analyses were performed on the centers and edges of the grains. All sites show a moderate to low content of common Pb (Table 3). The analyses have high Th/U ratios, mostly >1.0, which is typical for zircons grown from the late stage of crystallization of basic magma. The U-Pb ages are concordant within analytical errors and indicate a single age population (Fig. 8, Table 3). All analyses yield a concordia age of 1488 ± 4 Ma, with an MSWD of 0.57 (Fig. 8).

4.3. ^{40}Ar–^{39}Ar geochronology

Sample GD-456 is a fine-grained green granofels of the Nhunguara Formation and is composed of actinolite (44 vol. %), epidote (44%), brown hornblende (5%) and quartz (3%). Opaque minerals, plagioclase, apatite, titanite and sericite are accessory phases. The rock exhibits a relict igneous texture. Randomly orientated relict tabular plagioclase grains have been largely replaced by cryptocrystalline aggregates of epidote ± sericite. Domains rich in pseudomorphs of plagioclase alternate with actinolite-rich domains. In the latter, the actinolite is randomly oriented. Quartz preserves its igneous interstitial texture but shows patchy undulose extinction and an absence of recrystallization features, indicating low-temperature (< 300°C) deformation (e.g., Stipp et al., 2002; Faleiros et al., 2010). The brown hornblende is euhedral, shows oscillatory compositional zoning and is in disequilibrium with the metamorphic mineral assemblage, being partially replaced by actinolite aggregates. These features suggest that it is of igneous nature. Two grains of brown hornblende of the sample GD-456 were analyzed (Table 4), but only one grain produced a plateau age (1390 ± 20 Ma, Fig. 9), according to the definition of Fleck (1977). This age is inferred as the time of cooling of the rock below 500-450°C (the closure temperature of amphibole).

4.4. Sr–Nd whole-rock isotope data

The 14 Rb–Sr and Sm–Nd whole-rock analyses performed in the Votuverava metabasites include three samples of amphibolite lenses interbedded with the mica schists south of the Ribeira Shear Zone and 11 greenschist facies metabasites of the Rubuquara, Nhunguara and Piririca Formations north of the Ribeira Shear Zone (Fig. 2). The analytical results are shown in Table 5.

Initial $^{87}Sr/^{86}Sr$ ratios calculated for 1490 Ma vary from 0.69466 to 0.72579 (Table 5; Fig. 10a). The $\varepsilon_{Nd}(t)$ ranged from +0.10 to +3.55, with the exception of sample F-036, which had a value of -3.02 (Table 5; Fig. 10b). There is an incremental increase in $\varepsilon_{Nd}(t)$ from B1 to B3 and a negative correlation between $\varepsilon_{Nd}(t)$ and Sm/Nd (Table 5; Fig. 10b). The Sm-Nd T_{DM} model ages vary between 1640 and 2110 Ma, with an average value of 1760 Ma (Table 5).

5. Discussion

5.1. Element mobility and protolith controls on trace element and isotope geochemistry

There are no Votuverava Group mafic rocks free of metamorphism, and thus, element mobility cannot be quantified. Nonetheless, studies on mafic rocks affected by regional metamorphism indicate that the LILE abundances are strongly susceptible to modification, while the LREE abundances are generally weakly modified, and the HFSE and HREE contents are mostly unmodified (e.g., Becker et al., 1999, 2000; John et al., 2004; Tropper and Manning, 2005; Liu et al., 2007; Tang et al., 2007; Ker et al., 2014). In the MORB-normalized diagrams (Figs. 4-6), Cs, Rb, Sr, Ba, K and Pb show enrichment to depletion, while the Th, REEs and HFSEs display consistent behaviors. This pattern suggests that the LILE abundances were heterogeneously mobilized during metamorphism. Additional evidence for element mobility may be assessed using binary plots of mobile elements versus an immobile element (e.g., La). The plots of La versus Cs, Rb, Sr, Ba, K and Pb present no systematic correlation (Fig. 11a-f), corroborating the major mobility of these elements. Conversely, the plots of La versus Th, U, REE

and HFSE show strong positive correlations (Fig. 11g-l), suggesting that protolith abundances of these elements are largely preserved.

The Rb-Sr isotope system provides additional constraints on the element mobility. The initial $^{87}Sr/^{86}Sr$ ratios are strongly scattered (Table 5), as seen in the plot of initial $^{87}Sr/^{86}Sr$ versus $\varepsilon_{Nd(t)}$ (Fig. 10a), indicating that the Rb-Sr isotopic system was strongly modified by metamorphic processes. The Sm-Nd isotopic system displays a more coherent behavior (Fig. 10a-c), suggesting a major protolith control.

5.2. Tectonic setting of basic magmatism

The Votuverava metabasites present major element abundances within the range of tholeiitic basaltic compositions. However, as discussed above, the chemical data indicate post-magmatic modifications of the LILE abundances, so further interpretation is based on immobile trace elements. The distinction among the B1, B2 and B3 chemical groups of mafic rocks with respect to the Ti/V versus Nb/Yb ratios is evident (Fig. 3a). Depletion in V relative to Ti is a function of the oxygen fugacity of the magma and its source, the degree of partial melting and fractional crystallization (Shervais, 1982). Modeling of partial melting and fractional crystallization indicates that primary magmas producing 20 to 30% of the partial melting under reducing conditions, as in mid-ocean ridges, will result in a Ti/V between 20 and 50, whereas similar melts produced under more oxidizing conditions, as in subduction-related settings, will result in a Ti/V between 10 and 20. Alkaline basalts, such as ocean intraplate basalts, exhibit a Ti/V higher than 50 (Shervais, 1982). Basaltic rock associations with a Ti/V varying from 10 to 50, as is the case for the Votuverava metabasites, are observed in modern and ancient oceanic back-arc basin environments (Shervais, 1982; Leat et al., 2000;

Fretzdorff, 2002; Farahat, 2010). Shervais (1982) demonstrates that fractional crystallization of silicates does not significantly affect the Ti/V ratio, resulting in differentiation tendencies with near-constant Ti/V ratios. Conversely, the Ti/V ratio can be strongly affected by fractional crystallization of magnetite and/or hornblende, which may be identified by negative correlations between Si (or Zr) and Ti (or V) (Shervais, 1982). Because the analyzed samples show a strong positive correlation between TiO_2 and Zr (Fig. 3f), fractional crystallization of magnetite or hornblende should be disregarded. In this case, therefore, the Ti/V ratio can be considered a good tectonic discriminant.

In addition to the Ti/V ratios, the B1 samples present other characteristics of subduction-related magmas (Pearce et al., 1982; Pearce and Peat, 1995; Pearce and Stern, 2006; Pearce, 2008): (1) depleted HFSE contents relative to MORB abundances (Figs. 4-6); (2) a negative Nb-Ta anomaly relative to Th and La contents (Fig. 4-6), with Nb/Nb* values primarily between 0.2 and 0.7 (average of 0.6); and (3) enrichment in Th and U relative to MORB values. Furthermore, the relationships between non-conservative/conservative trace element ratios (e.g., Ta/Yb versus Th/Yb, Ce/Nb versus Th/Nb, Th/Yb versus Nb/Yb; Fig. 12) of the Votuverava metabasites are similar to those of subduction-related oceanic basalts, suggesting a variable contribution of the subduction component to the magma source (Pearce et al., 1982; Pearce and Peate, 1995; Pearce and Stern, 2006; Pearce, 2008). The B1 and B2 trace element behaviors are very similar to the patterns found in modern oceanic back-arc basin basalts (BBABs) (e.g., East Scotia Ridge, Leat et al., 2000; Fretzdorff et al., 2002) (Figs. 4 and 5). Metabasalts with preserved igneous hornblende (e.g., sample GD-456, this work; Maniesi, 1997) also corroborate the existence of subduction-related environments,

where slab-related hydrous fluids contribute to the magma (e.g., Barclay and Carmichael, 2004).

The overall chemical patterns of the B2 and B3 groups are similar to transitional and enriched MORB patterns, respectively, possibly with a contribution of a subduction-related component. The existence of metabasic rocks with chemical signatures transitional to MORB and arc-related basalts as well as the large variation in Ti/V ratios (9-41) strongly suggest a back-arc basin environment for the Votuverava Group basic magmatism.

Available elemental and isotopic data (Figs. 4b,f, 10, 12; Siga Jr. et al., 2011b) indicate that metabasites from the Betara Formation (~50 km southwest of the study area; Fig. 1) present a B1 group chemical signature. This reinforces the existence of an extensive oceanic back-arc basic magmatism recorded in the southern Ribeira Belt.

5.3. Melt sources

The mostly positive initial ε_{Nd} values and T_{DM} model ages of 1640-2110 Ma suggest a major contribution of juvenile mantle sources with a minor and variable participation of reworked older crustal material. Sm-Nd data presented by Siga Jr. et al. (2011a,b) (ε_{Nd} from -3 to +6 and T_{DM} model ages between 1500 and 2100 Ma) for samples of the Perau and Betara Formations are consistent with our data (Fig. 10a,b). The strong negative correlation between Sm/Nd and ε_{Nd} (Fig. 10b) is evidence of a heterogeneous contribution of different melt sources to the Votuverava Group mafic magmatism.

The relationships between the Nb/Yb and TiO_2/Yb ratios suggest that the B1 and B2 samples were generated by shallow melting (Fig. 12a; Pearce and Peate, 1995;

Pearce and Stern, 2006; Pearce, 2008). This compositional pattern is expected and observed in mid-ocean ridge basalts and in subduction-related basalts (e.g., Pearce and Peate, 1995; Pearce and Stern, 2006; Pearce, 2008). Conversely, the B3 samples display Ti contents slightly higher than the mantle array (Fig. 12a), suggesting a deeper melting, which could suggest plume interactions (Pearce, 2008). The Nb/Yb ratios also indicate progressively more fertile mantle sources from B1 to B3 (Fig. 12a,b).

The overall compositional distribution of the Votuverava metabasites is similar to the geochemical patterns found in modern environments of mid-ocean ridges interacting with plumes, such as the Galapagos System, the Iceland-Reykjanes Ridge System and the South American-Antarctica Ridge (Pearce, 2008 and references therein). A very similar pattern is found in basalts from the East Scotia Ridge oceanic back-arc basin (Fig. 12a-d), which interacts with a plume associated with Bouvet Island (Leat et al., 2000; Fretzdorff et al., 2002). Part of the Votuverava metabasites display Th/Yb ratios higher than the mantle array (Fig. 12b,c), consistent with a variable contribution of the subduction component to the source of the magmatism. The overall geochemical distribution is consistent with a partial association with a subduction component and MORB-type mantle sources and with MORB-type and plume mantle sources. The LILE mobility during metamorphism precludes distinguishing whether the subduction component is dominated by slab-derived fluid or subducted sediment because elements that are abundant in slab-derived fluids (Cs, Ba, Rb, K, Pb, Sr) are more mobile during metamorphism.

5.4. Age of the basic magmatism

Considering the general difficulty in dating mafic rocks by the zircon U-Pb method, the significance of the concordia age of 1488 ± 4 Ma obtained for the GI-7C sample (B1 group) should be discussed. Fourteen U-Pb SHRIMP analyses performed on 14 zircon grains were used in the calculation of the concordia age. Analytically, therefore, the age is of high quality. Conversely, it is necessary to demonstrate whether this age represents the time of the igneous protolith crystallization, inheritance or a metamorphic age.

The third hypothesis should be disregarded because there are no metamorphic zircon overgrowths, and petrographic evidence indicates that the GI-7C sample was affected by lower greenschist facies metamorphism. Several lines of evidence favor the first hypothesis: (1) the analyzed zircon grains are xenomorphic, and there are no rounded (typical of detrital or resorbed xenocrystic) grains (Fig. 7); (2) the dominant textural characteristics of the dated zircon grains, with unzoned or poorly zoned grains (grains 1, 2, 4, 5, 6, 8, 9, 11, 12, Fig. 7) and grains with sector zoning (grains 3 and 13, Fig. 7), are typical of zircon from mafic rocks; (3) there are no prismatic zircon grains with well-defined oscillatory zoning typical of felsic magmas; (4) a single-age population is unexpected for inherited detrital or xenocrystic zircon grains; (5) available zircon U-Pb (SHRIMP and ID-TIMS) data for mafic rocks from the Votuverava Group (Fig. 2; Siga Jr. et al., 2011a) and the Betara Formation (Siga Jr. et al., 2011b) yielded average ages ranging from 1451 to 1489 Ma, which are, within errors, consistent with the data from sample GI-7C; and (6) there is no detrital zircon population of ca. 1490 Ma in the metasedimentary host rocks, which are largely dominated by zircon ages ≥ 2000 Ma (Basei et al., 2008; Campanha et al., 2009, 2010; Faleiros et al., 2012, 2015; Faleiros and Pavan, 2013). Thus, the concordia age of 1488 ± 4 Ma is best interpreted as an igneous protolith crystallization age.

Elemental and isotopic data (Figs. 4b,f, 10, 12; Siga Jr. et al., 2011a,b) suggest that all available zircon U-Pb ages come from metabasites with B1 group (BABB-like) chemical signatures. Nonetheless, with the currently available geochronological data, it is not possible to assign different ages to the subunits of the Votuverava Group because B1 rocks occur in all subunits. Thus, we contend that it is most likely that they are related to the same overall ca. 1490 Ma age, as suggested by all available zircon U-Pb data (this work; Siga Jr. et al., 2011a,b). Similar zircon U-Pb ages of ca. 1500 Ma were also reported for metabasic rocks from the Água Clara Formation (Fig. 1b) (Weber et al., 2004). Chemical data indicate that the Água Clara Formation metabasites also have BABB-like signatures (Maniesi, 1997), corroborating extensive Calymmian back-arc basin magmatism in the southern Ribeira Belt.

The hornblende ^{40}Ar–^{39}Ar age of 1390 ± 20 Ma obtained for the GD-456 sample (B3 group) is approximately 100 Ma younger than the zircon U-Pb ages obtained for the Votuverava samples (this work; Siga Jr. et al., 2011a,b). This indicates the closure temperature age for ^{40}Ar–^{39}Ar in hornblende (500-450 °C).

The Sm–Nd results obtained from the Votuverava metabasites plotted in a ^{143}Nd–^{144}Nd versus ^{147}Sm–^{144}Nd diagram mostly form a linear array with a slope equivalent to 1225 Ma ± 68 Ma (MSWD=8.4) (Fig. 10c). This apparent age is approximately 270 million years younger than the zircon U-Pb ages and cannot represent the igneous crystallization. As discussed above, the REE abundances were mostly unmodified during metamorphism, and thus, this apparent age cannot reflect a metamorphic event. Geochemical and Nd isotopic data indicate that the Votuverava metabasites show heterogeneous sources, and therefore, it is improbable that all of the samples had the same initial $^{143}Nd/^{144}Nd$ isotopic ratios. Thus, the slope in the $^{147}Sm/^{144}Nd$ –$^{143}Nd/^{144}Nd$ space might reflect a mixing line of no age significance due to different source

components for the basic magmatism, as described by Chauvel et al. (1985) and Friend et al. (2009). In similar cases, depending on the nature of the mixing components, the apparent age may be too older (Chauvel et al., 1985) or too younger (Friend et al., 2009) than the igneous crystallization age.

5.5. Regional geotectonic implications

Geological mapping and available U-Pb geochronological data (this work; Juliani et al., 2000; Weber et al., 2004; Siga Jr. et al., 2011a,b; Faleiros et al., 2012, 2015; Faleiros and Pavan, 2013; Henrique-Pinto et al., 2014) demonstrate the existence of a 500-km-long and 60-km-wide belt composed essentially of ca. 1400-1500 Ma Mesoproterozoic units in the southern and central domains of the Ribeira Belt (Fig. 1b). The age at which this terrane was last a coherent block is still uncertain, primarily due to an intense overprint of Neoproterozoic orogenic metamorphism and deformation (Juliani et al., 2000; Faleiros et al., 2010, 2011a). The geological, geochemical and geochronological data presented in this work, in conjunction with available data (Maniesi, 1997; Weber et al., 2004; Siga Jr. et al., 2011a,b), suggest the existence of extensive ca. 1490 Ma oceanic back-arc basic magmatism recorded in the southern Ribeira Belt.

In a global perspective, a basic magmatism of ca. 1500-1450 Ma age is reported worldwide in Paleoproterozoic cratonic fragments, as in the São Francisco Craton in Brazil (Silveira et al., 2013) and its African counterpart (Congo Craton) in Angola (Ernst et al., 2012), the Siberia Craton (Ernst et al., 2000, 2008), the Tarim Craton in northwestern China (Wu et al., 2014), the Yangtze Block in southern China (Fan et al., 2013), the Bastar Craton of India (Pisarevsky et al., 2013) and in Baltica (Lubnina et al.,

2010). Some of these occurrences were used as evidence for the Columbia configuration of Lubnina et al. (2010) and Silveira et al. (2013), while others inferred this as extensional intracratonic magmatism associated with the breakup of Columbia (e.g., Fan et al., 2013; Wu et al., 2014). Geological, geochronological and Hf isotope data of detrital zircon grains from around the world support the interpretation that the Columbia supercontinent remained a quasi-integral entity throughout the period of 1800-1300 Ma (Roberts, 2012, 2013). Hf data in the detrital zircons indicate largely juvenile signatures during the 1700-1300 Ma period, indicating a dominance of accretionary orogens related to plate margins (Roberts, 2012, 2013). During the Ediacaran (West Gondwana time), this Mesoproterozoic belt was located between the Paranapanema and Congo Cratons, apparently as an exotic terrane (*sensu* Howell, 1995). The Paranapanema Craton is completely covered by Paleozoic sedimentary rocks from the Paraná Basin (Fig. 1a) and was recognized by data from deep boreholes and geophysical studies (Mantovani and Brito Neves, 2005), precluding detailed studies to reveal its geotectonic relationships.

The existence of the Calymmian belt in the Ribeira Belt raises the possibility of records of orogenic activity older than the Neoproterozoic Brasiliano-Pan African cycle. Available Rb–Sr ages obtained in rocks from the Votuverava Group are 1212 + 55 Ma (Batolla Jr. et al.,1981, Teixeira, 1982) and 1283 ± 28 Ma (Daitx, 1996). Recently, a ^{40}Ar–^{39}Ar age of 1120 ± 70 Ma was obtained from muscovite grains present in a subhorizontal S_1 slate cleavage of a Votuverava phyllite (Cury et al., 2008). These ages suggest the presence of a Grenvillian-age tectono-metamorphic event in the southern part of the Ribeira Belt. Additionally, a ca. 1100 Ma inheritance has been recognized in zircon grains from Ediacaran granites intrusive in the Embu Terrane (Alves et al., 2013), a unit adjacent to the Votuverava Group (Fig. 1b). Speculatively, the available

data could indicate that the ca. 1490 Ma Votuverava Group back-arc system could have been involved in a 1280-1100 Ma collisional orogeny related with the Rodinia assembly, as reported from elsewhere in the world (Roberts, 2013).

6. Conclusions

(1) Metabasic rocks in the Votuverava Group are derived in part from volcanism and in part from coeval intrusions and are largely basaltic in composition.

(2) SHRIMP U-Pb zircon geochronology on a metabasic sample yielded high Th/U magmatic zircons with an age of 1488 ± 4 Ma, which is interpreted as the time of igneous crystallization.

(3) Sm–Nd results obtained from metabasites plotted in a ^{143}Nd–^{144}Nd versus ^{147}Sm–^{144}Nd diagram mostly form a linear array with a slope of 1225 Ma, which is interpreted as a mixing line of no age significance that is related to different source components for the metabasic rocks.

(4) The trace element and Nd-Sr isotopic chemistry of the metabasic rocks suggests that they were most likely emplaced into a back-arc environment. Essentially positive $\varepsilon_{Nd(t)}$ values (+0.10 to +3.55) suggest a dominant juvenile mantle source to the basic magmatism.

(5) The 1490 Ma mafic magmatism is associated with a 500-km-long and 60-km-wide Calymmian belt interpreted as the back-arc component of an accretionary orogen.

(6) The available thermochronological data suggest that the ca. 1490 Ma Votuverava Group was involved in a 1280-1100 Ma collisional orogeny, possibly related to the Rodinia assembly.

Acknowledgments

Financial support was provided by FAPESP (Fundação de Amparo à Pesquisa do Estado de São Paulo – Brazil) grants 96/05648-1, 01/13457-1 and 06/01327-00. APN acknowledges research support from the Chinese Academy of Geological Sciences and the GeoQuEST Research Centre at the University of Wollongong. Two anonymous reviewers provided insightful and helpful comments that improved the resulting contribution. Editor Guochun Zhao is thanked for his guidance during the editorial process.

References

Alves, A., Janasi, V.A., Campos Neto, M.C., Heaman, L., Simonetti, A., 2013. U–Pb geochronology of the granite magmatism in the Embu Terrane: Implications for the evolution of the Central Ribeira Belt, SE Brazil. Precambrian Research 230, 1–12.

Barclay, J., Carmichael, I.S.E., 2004. A Hornblende Basalt from Western Mexico: Water-saturated Phase Relations Constrain a Pressure-Temperature Window of Eruptibility. Journal of Petrology 45, 485–506.

Basei, M.A.S., Frimmel, H.E., Nutman, A.P., Preciozzi, F., 2008. West Gondwana amalgamation based on detrital zircon ages from Neoproterozoic Ribeira and Dom Feliciano Belts of South America and comparison with coeval sequences from SW Africa. Geological Society Special Publications 294, pp. 239–256.

Batolla Jr., F.; Silva, A.T.S.F.; Algarte, J.P. 1981. O Pré-Cambriano da Região Sul-Sudeste do Estado de São Paulo e Este-Nordeste do Estado do Paraná. In: Simpósio Regional de Geologia, 3, Curitiba, 1981. Atas... São Paulo, SBG. v.1, p. 94–108.

Becker, H., Jochum, K.P., Carlson, R.W., 1999. Constraints from high-pressure veins in eclogites on the composition of hydrous fluids in subduction zones. Chemical Geology 160, 291–308.

Becker, H., Jochum, K.P., Carlson, R.W., 2000. Trace element fractionation during dehydration of eclogites from high-pressure terranes and the implications for element fluxes in subduction zones. Chemical Geology 163, 65–99.

Bettencourt, J.S., Leite Jr., W.B., Ruiz, A.S., Matos, R., Payolla, B.L., Tosdal, R.M., 2010. The Rondonian-San Ignacio Province in the SW Amazonian Craton: An overview. Journal of South American Earth Sciences 29, 28–46.

Bigarella, J.J & Salamuni, R. 1958. Estudos preliminares na Série Açungui. VIII. A Formação Votuverava. Curitiba, Instituto de História Natural, 6 p. (Boletim. Geologia, 2).

Boynton, W.V., 1984. Cosmochemistry of the rare earth elements: meteorite studies. In: Henderson, P. (ed) Rare Earth Element Geochemistry. Elsevier, Amsterdam, p. 63–114.

Campanha, G.A.C., 1991. Tectônica Proterozóica no Alto e Médio Vale do Ribeira, Estados de São Paulo e Paraná. Tese de Dourorado, Instituto de Geociências da Universidade de São Paulo, 296 p., anexos.

Campanha, G.A.C., 2002. O papel do sistema de zonas de cisalhamento transcorrentes na configuração da porção meridional da Faixa Ribeira. Tese de Livre-Docência, Instituto de Geociências da Universidade de São Paulo, 105 p., 5 anexos.

Campanha, G.A.C., Brito Neves, B.B., 2004. Frontal and oblique tectonics in the Brazilian shield. Episodes 27, 255–259.

Campanha, G.A.C., Faleiros, F.M., 2005. Neoproterozoic terrane collage in the southern and central Ribeira Belt, Brazil. In: Gondwana 12 Conference: Geological and

Biological Heritage of Gondwana, Mendoza, 2005. Abstracts... Mendoza: National Academy of Sciences (Argentina), v. 1, p. 81.

Campanha, G.A.C., Sadowski, G.R. 1999 Tectonics of the Southern Portion of the Ribeira Belt (Apiaí Domain). Precambrian Research 98, 31–51.

Campanha, G.A.C., Basei, M.S., Tassinari, C.C., Nutman, A.P., Faleiros, F.M., 2008. Constraining the age of the Iporanga Formation with SHRIMP U-Pb zircon: implications for possible Ediacaran glaciation in the Ribeira Belt, SE Brazil. Gondwana Research 13, 117–125.

Campanha, G.A.C., Basei, M.A.S.; Faleiros, F.M.; Tassinari, C.C.G.; Nutman, A.P.; Vasconcelos, P.M.; Dantas, E.L., 2009. Geocronologia do Terreno Apiaí no Sul do Estado de São Paulo. In: 45 Anos de Geocronologia no Brasil, 2009, São Paulo. Boletim de Resumos Expandidos. São Paulo: IGc-USP. p. 220–221.

Campanha, G.A.C.; Gimenez Filho, A.; Caetano, S.L.V.; Pires, F.A.; Dantas, A.S.L.; Teixeira, A.L.; Dehira, L.K. 1986. Geologia e estratigrafia da região das folhas Iporanga e Gruta do Diabo, Vale do Ribeira, São Paulo. In: Congresso Brasileiro de Geologia, 34, Goiânia, 1986. Anais... Goiânia, SBG. v. 2, p. 1058–1073.

Campos Neto, M.C. 1983. Contribuição à litoestratigrafia do Grupo Açungui no sudeste do Estado de São Paulo. In: Simpósio Regional de Geologia, 4, São Paulo, 1983. Atas... São Paulo, SBG. p.103–112.

Chiodi Filho, C. 1984. Contribuição à geologia das regiões sul paulista e leste paranaense, Grupos Açungui e Setuva. In: Congresso Brasileiro de Geologia, 33, Rio de Janeiro, 1984. Anais... Rio de Janeiro, SBG. v.5, p. 2394–2406.

Cordani, U.G., Fraga, L.M., Reis, N., Tassinari, C.C.G., Brito-Neves, B.B., 2010. On the origin and tectonic significance of the intra-plate events of Grenvillian-type age

in South America: A discussion. Journal of South American Earth Sciences 29, 143–159.

Cumming, G.L., Richards, J.R., 1975. Ore lead isotope ratios in a continuously changing earth. Earth and Planetary Science Letters 28, 155-171.

Cury, L.F., 2009. Geologia do Terreno Paranaguá. Tese de Doutorado, Instituto de Geociências, Universidade de São Paulo.

Cury, L.F., Kaulfuss, G.A., Siga Jr., O., Basei, M.A.S., Harara, O.M.M., Sato, K., 2002. Idades U–Pb (zircões) de 1,75 Ga em Granitóides Alcalinos Deformados dos Núcleos Betara e Tigre: Evidências de Regimes Extensionais do Estateriano na Faixa Apiai. Geologia USP–Série Científica 2, 95–108.

Cury, L.F., Siga Jr., O., Harara, O.M.M., Prazeres Filho, H.J., Basei, M.A.S., 2008. Aspectos Tectônicos das Intrusões dos Granitos do Cerne, Passa Três e Rio Abaixo, Sudeste do Pré-cambriano Paranaense. Estudo Baseado em Datações ^{39}Ar-^{40}Ar em Micas.. Geologia USP. Série Científica 8, 87–104.

Daitx, E.C., 1996. Origem e evolução dos depósitos sulfetados tipo Perau (Pb-Zn-Ag), com base nas jazidas de Canoas e Perau (Vale doRibeira, PR). Rio Claro, UNESP, 453p. (PhD. thesis).

Dürr, S.B., Dingeldey, D.P., 1996. The Kaoko belt (Namibia): part of a late Neoproterozoic continental-scale strike-slip system. Geology 24, 503–506.

Egydio-Silva, M., Vauchez, A., Bascou, J., Hippertt, J., 2002. High-temperature deformation in the Neoproterozoic transpressional Ribeira belt, southeast Brazil. Tectonophysics 352, 203–224.

Elliott, T., Plank, T., Zindler, A., White, W., Bourdon, B., 1997. Element transport from slab to volcanic front at the Mariana arc. Journal of Geophysical Research 102, 14991–15019.

Ernst, R.E., Buchan, K.L., Hamilton, M.A., Okrugin, A.V., Tomshin, M.D., 2000. Integrated paleomagnetism and U–Pb geochronology of mafic dikes of the Eastern Anabar Shield Region, Siberia: implications for the Mesoproterozoic paleolatitude of Siberia and comparison with Laurentia. Journal of Geology 108, 381–401.

Ernst, R.E., Hamilton, M.A., Pereira, E., Rodrigues, J., Tassinari, C., Van-Dunem, V., 2012. Intraplate magmatic 'barcode' record of the Congo craton (Angola portion): newly dated dolerite events at 1502 and 1100 Ma and implications for Nuna and Rodinia supercontinental reconstructions. Abstract 35, Geological Association of Canada (GAC) — Mineralogical Association of Canada (MAC) Joint Annual Meeting — Geoscience at the Edge, May 27–29, 2012, St. John's, Newfoundland and Labrador, Canada.

Ernst, R., Wingate, M., Buchan, K.L., Li, Z.X., 2008. Global record of 1600–700 Ma LargeIgneous Provinces (LIPs): implications for the reconstruction of the proposedNuna (Columbia) and Rodinia supercontinents. Precambrian Research 160, 159–178.

Faleiros, F.M., 2003. Zona de Cisalhamento Ribeira: deformação, metamorfismo e termobarometria de veios sin-tectônicos. Dissertação de Mestrado, Instituto de Geociências, Universidade de São Paulo, 147 p.

Faleiros, F.M., 2008. Evolução de terrenos tectono-metamórficos da Serrania do Ribeira e Planalto Alto Turvo (SP, PR). Tese de Doutorado, Instituto de Geociências, Universidade de São Paulo, 306 p.

Faleiros, F.M., Campanha, G.A.C., 2004. Petrografia e microestruturasde tectonitos da Zona de Cisalhamento Ribeira, Vale do Ribeira, SP e PR: implicações no zoneamento metamórfico e estrutural do Supergrupo Açungui e unidades correlatas. Revista Brasileira de Geociências 34, 419–430.

Faleiros, F.M., Pavan, M., 2013. Geologia e recursos minerais da folha Eldorado Paulista – SG.22-X-B-VI, Estado de São Paulo, Escala 1:100.000 São Paulo: Programa Geologia do Brasil, CPRM-Serviço Geológico do Brasil. 128 p.

Faleiros, F. M., Campanha, G.A.C., Bello, R. M. S., Fuzikawa, K., 2007. Fault-valve action and vein development during strike-slip faulting: an example from the Ribeira Shear Zone, Southeastern Brazil. Tectonophysics 438, 1–32.

Faleiros, F. M., Campanha, G.A.C., Bello, R. M. S., Fuzikawa, K., 2010. Quartz recrystallization regimes, c-axis texture transitions and fluid inclusion reequilibration in a prograde greenschist to amphibolite facies mylonite zone (Ribeira Shear Zone, SE Brazil). Tectonophysics 485, 193–214.

Faleiros, F.M., Campanha, G.A.C, Martins, L., Vlach, S.R.F., Vasconcelos, P.M., 2011a. Ediacaran high-pressure collision metamorphism and tectonics of the southern Ribeira Belt: evidence for terrane accretion and dispersion during Gondwana assembly. Precambrian Research 189, 263–291.

Faleiros, F.M., Ferrari, V.C., Costa, V.S., Campanha, G.A.C., 2011b. Geoquímica e petrogênese de metabasitos do Grupo Votuverava (Terreno Apiaí, Cinturão Ribeira Meridional): Evidências de uma bacia retroarco calimiana. Geologia USP–Série Científica 11, 135–155.

Faleiros, F.M., Morais, S. M., Costa, V. S., 2012. Geologia e Recursos Minerais da Folha Apiaí - SG.22-X-B-V - Estados de São Paulo e Paraná, escala 1:100.000. 1. ed. São Paulo: Programa Geologia do Brasil, CPRM-Serviço Geológico do Brasil. 107 p.

Faleiros, F.M., Pavan, M., Caltabeloti, F.P., Pinto, L.G.R., 2015. Programa Geologia do Brasil, Levantamentos Geológicos Básicos. Capão Bonito – Folha SG.22-X.B.III, escala 1:100.000, Estado de São Paulo. Carta Geológica.

Fan, H.-P., Zhu, W.-G., Li, Z.-X., Zhong, H., Bai, Z.-J., He, D.-F., Chen, C.-J., Cao, C.-Y., 2013. Ca. 1.5 Ga mafic magmatism in South China during the break-up of the supercontinent Nuna/Columbia: The Zhuqing Fe–Ti–V oxide ore-bearing mafic intrusions in western Yangtze Block. Lithos 168–169, 85–98.

Fan, W., Wang, Y., Zhang, A., Zhang, F., Zhang, Y., 2010. Permian arc–back-arc basin development along the Ailaoshan tectonic zone: Geochemical, isotopic and geochronological evidence from the Mojiang volcanic rocks, Southwest China. Lithos 119, 553–568.

Farahat, E.S., 2010. Neoproterozoic arc–back-arc system in the Central Eastern Desert of Egypt: Evidence from supra-subduction zone ophiolites. Lithos 120, 293–308.

Fiori, A.P., 1992. Tectônica e estratigrafia do Grupo Açungui, PR. Boletim IG-USP 23, 55–74.

Fleck, R.J., Sutter, J.F., Elliot, D.H., 1977. Interpretation of discordant 40Ar/39Ar age-spectra of Mesozoic tholeiites from Antarctica. Geochimica et Cosmochimica Acta 41, 15–32.

Frascá, M.B.H.O., Campanha, G.A.C., Figueiredo, M.C.H., Sadowski, G.R., 1997. Geoquímica e ambiência tectônica de metabasitos do alto e médio Vale do Ribeira, São Paulo e Paraná. Revista Brasileira de Geociências 27, 41–48.

Fretzdorff, S., Livermore, R.A., Devey, C.W., Leat, P.T., Stoffers, P., 2002. Petrogenesis of the Back-arc East Scotia Ridge, South Atlantic Ocean. Jornal of Petrology 43, 1435–1467.

John, T., Scherer, E.E., Haase, K., Schenk, V., 2004. Trace element fractionation during fluidinduced eclogitization in a subducting slab: trace element and Lu–Hf–Sm–Nd isotope systematics. Earth and Planetary Science Letters 227, 441–456.

Hackspacher, P.C., Dantas, E.L., Spoladore, A., Fetter, A.H., Oliveira, M.A.F., 2000. Evidence for Neoproterozoic backarc basin development in the central Ribeira Belt, southeastern Brazil: new geochronological and geochemical constraints from the São Roque-Ac¸ungui groups. Revista Brasileira de Geociências 30, 110–114.

Heilbron, M., Pedrosa-Soares, A.C., Campos Neto, M.C., Silva, L.C., Trouw, R.A.J., Janasi, V.A., 2004. Província Mantiqueira. In: Mantesso-Neto, V., Bartorelli, A., Carneiro, C.D.R., Brito-Neves, B.B. (Eds.), Geologia do Continente Sul-Americano: Evolução da Obra de Fernando Flávio Marques de Almeida, pp. 203–234.

Henrique-Pinto, R., Janasi, V.A., Vasconcellos, A.C.B.C., Sawyer, E.W., Barnes, S.-J., Basei, M.A.S., Tassinari, C.C.G., 2015. Zircon provenance in meta-sandstones of the São Roque Domain: Implications for the Proterozoic evolution of the Ribeira Belt, SE Brazil. Precambrian Research 256, 271–288.

Howell, G.H., 1995. Principles of Terrenes Analysis: New Applications for Global Tectonics. Chapman & Hall, London – Glasgow – Weinheim – New York – Tokyo – Melbourne – Madras, 245 p.

Irvine, T., Baragar, W., 1971. A guide to the chemical classification of the commonvolcanic rocks. Canadian Journal of Earth Sciences 8, 523–548.

Janasi, V.A., Leite, R.J., Van Schmus, W.R. 2001. U-Pb ages and chronostratigraphy of the granitic magmatism in the Agudos Grandes batholith (W of Sao Paulo, Brazil) – implications for the evolution of the Ribeira Belt. Journal of South American Earth Sciences 14, 363–376.

Janousek, V., Farrow, C. M., Erban, V., 2006. Interpretation of whole-rock geochemical data in igneous geochemistry: introducing Geochemical Data Toolkit (GCDkit). Journal of Petrology 47, 1255–1259.

Janousek, V., Farrow, C.M., Erban, V., Trubac, J., 2011. Brand new Geochemical Data Toolkit (GCDkit 3.0) - is it worth upgrading and browsing documentation? (Yes!). Geologicke vyzkumy na Morave a ve Slezsku 18, 26–30.

Jian, P., Liu, D.Y., Sun, X.M., 2008. SHRIMP dating of the Permo-Carboniferous Jinshajiang ophiolite, southwestern China: geochronological constraints for the evolution of Paleo-Tethys. Journal of Asian Earth Sciences 32, 371–384.

Jian, P., Liu, D.Y., Kröner, A., Zhang, Q., Wang, Y.Z., Sun, X.M., Zhang, W., 2009a. Devonian to Permian plate tectonic cycle of the Paleo-Tethys Orogen in southwest China (I): Geochemistry of ophiolites, arc/back-arc assemblages and within-plate igneous rocks. Lithos 113, 748–766.

Jian, P., Liu, D.Y., Kröner, A., Zhang, Q., Wang, Y.Z., Sun, X.M., Zhang, W., 2009b. Devonian to Permian plate tectonic cycle of the Paleo-Tethys Orogen in southwest China (II): Insights from zircon ages of ophiolites, arc/back-arc assemblages and within-plate igneous rocks and generation of the Emeishan CFB province. Lithos 113, 767–784.

Juliani, C.; Hackspacher, P.; Dantas, E.L.; Fetter, A.H., 2000. The Mesoproterozoic volcano-sedimentary Serra do Itaberaba Group of the central Ribeira Belt, São Paulo, Brazil: implications for the age of the overlying São Roque Group. Revista Brasileira de Geociências 30, 82–86.

Ker, C.-M., Yang, H.-J., Zhang, J., Shau, Y.-H., Chieh, C.-J., Meng, F., Takazawa, E., You, C.-F., 2014. Compositional and Sr–Nd–Hf isotopic variations of Baijingsi eclogites from the North Qilian orogen, China: Causes, protolith origins, and tectonic implications. Gondwana Research (2014), http:/dx.doi.org/10.1016/j.gr.2014.06.006.

Le Bas, M.J., Le Maitre, R.W., Streckeisen, A., Zanettin, B., 1986. A chemical classification of volcanic rocks based on the total alkali-silica diagram. Journal of Petrology 27, 745–750.

Leat, P.T., Livermore, R.A., Millar, I.L., Pearce, J.A., 2000. Magma supply in back-arc spreading centre segment E2, East Scotia Ridge. Journal of Petrology 41, 845–866.

Leonardos, O.H., 1934. Nota sobre a geologia do distrito de Iporanga. SP. Rio de Janeiro. DNPM Report 564.

Li, Z.X., Bogdanova, S.V., Davidson, A., Collins, A.S., De Waele, B., Ernst, R.E., Fitzsimons, I.C.W., Fuck, R.A., Gladkochub, D.P., Jacobs, J., Karlstrom, K.E., Lu, S., Natapov, L.M., Pease, V., Pisarevsky, S.A., Thrane, K., Vernikovsky, V., 2008. Assembly, configuration, and break-up history of Rodinia: A synthesis. Precambrian Research 160, 179–210.

Liu, Y.-H., Yang, H.-J., Shau, Y.-H., Meng, F.-C., Zhang, J.-X., Yang, J.-S., Xu, Z.-Q., Yu, S.-C., 2007. Compositions of high Fe–Ti eclogites from the Sulu UHP metamorphic terrane, China: HFSE decoupling and protolith characteristics. Chemical Geology 239, 64–82.

Lubnina, N.V., Mertanen, S., Söderlund, U., Bogdanova, S., Vasilieva, T.I., Frank-Kamenetsky, D., 2010. A new key pole for the East European Craton at 1452 Ma: palaeomagnetic and geochronological constraints from mafic rocks in the Lake Ladoga region (Russian Karelia). Precambrian Research 183, 442–462.

Ludwig, K.R., 2003. Isoplot 3.00: A Geochronological Toolkit for Microsoft Excel. Berkeley, California, Berkeley Chronology Center Special Publication No. 4.

Maniesi, V. 1997. Petrologia das rochas anfibolíticas das regiões de Adrianópolis, Campo Largo e Rio Branco do Sul/PR. 1997. 215 f. Tese (Doutorado) - Instituto de Geociências e Ciências Exatas, Universidade Estadual Paulista, Rio Claro.

Mantovani, M.S.M., Brito Neves, B.B., 2005. The Paranapanema lithospheric block: its importance for Proterozoic (Rodinia, Gondwana) supercontinent theories. Gondwana Research 8, 303–315.

McCulloch, M.T., Kyser, T.H., Woodhead, J.D., Kinsley L., 1994. Pb-Sr-Nd-O isotopic constraints on the origin of rhyolites from the Taupo Volcanic Zone of New Zealand: Evidence for assimilation followed by fractionation from basalt. Contributions to Mineralogy and Petrology 115, 303–312.

Metal Mining Agency Of Japan. Japan International Cooperation Agency. 1981. Report on geological survey of Anta Gorda; phase 1. Convênio DNPM/MMAJ/JICA. (unpublished report)

Metal Mining Agency Of Japan. Japan International Cooperation Agency. 1982. Report on geological survey of Anta Gorda; phase 2. Convênio DNPM/MMAJ/JICA. (unpublished report)

Metal Mining Agency of Japan. Japan International Cooperation Agency. 1983. Report on geological survey of Anta Gorda; phase 3 Convênio DNPM/MMAJ/JICA. (unpublished report)

Miyashiro, A., 1961. Evolution of metamorphic belts. Journal of Petrology 2, 277–311.

Miyashiro, A., 1973. Metamorphism and Metamorphic Belts. Londres: George Allen & Unwin. 492 p.

Nogueira, S.A.A. 1990. Estudo das mineralizações filoneanas auríferas do depósito de Piririca, Vale do Ribeira, SP. São Paulo. 91 p. (MSc. dissertation, Instituto de Geociências da Universidade de São Paulo).

Paces, J.B., Miller, J.D.L., 1993. Precise U-Pb ages of Duluth Complex and related mafic intrusions, northeastern Minnesota: geochronological insights to physical,

petrogenetica, paleomagnetic, and tectonomagmatic processes associated with the 1.1 Ga midcontinent rift system. Journal of Geophysical Research 98, 13997–134013.

Passarelli, C.R., Basei, M.A.S., Campos Neto, M.C., Siga Jr., O., Prazeres Filho, H.J., 2004. Geocronologia e geologia isotópica dos terrenos Pré-Cambrianos da porção sul-oriental do Estado de São Paulo. Geologia USP–Série Científica 4, 55–74.

Pearce, J.A., 1982. In: Thorpe, R.S. (Ed.), Trace Element Characteristics of Lavas from Destructive Plate Boundaries. John Wiley and Sons, Andesites, pp. 525–548.

Pearce, J.A., 1983. Role of the sub-continental lithosphere in magma genesis at active continental margins. In: Hawkesworth, C.J. and Norry, M.J. (eds.), Continental basalts and mantle xenoliths. Shiva, Nantwich, p. 230–249.

Pearce, J.A., 2008. Geochemical fingerprinting of oceanic basalts with applications to ophiolite classification and the search for Archean oceanic crust. Lithos 100, 14–48.

Pearce, J.M., Peate, D.W., 1995. Tectonic implications of the composition of volcanic arc magmatism. Annual Review of Earth and Planetary Sciences 23, 251–285.

Pearce, J.A., Stern, R.J., 2006. Origin of backarc basin magmas: trace element andisotope perspectives. In: Back-Arc Spreading Systems: Geological, Biological,Chemical, and Physical Interactions., pp. 63–86.

Pearce, J.A., Ernewein, M., Bloomer, S.H., Parson, L.M., Murton, B.J., Johnson, L.E., 1994. Geochemistry of Lau Basin volcanic rocks: influence of ridge segmentation and arc proximity. In: Smellie, J.L. (Ed.), Volcanism Associated with Extension at Consuming Plate Margins. Geological Society Special Publication 81, 53–75.

Perrota, M.M., 1996. Potencial aurífero de uma região no Vale do Ribeira, São Paulo, estimado por modelagem de dados geológicos, geoquímicos e geofísicos num sistema de informações georreferenciadas. São Paulo, 90 p. (Ph. D. thesis, Instituto de Geociências da Universidade de São Paulo).

Piekarz, G.F., 1981. Reconhecimento das Unidades correlacionáveis à seqüência mineralizada do Perau - Estado do Paraná. In: Simpósio Regional de Geologia, 3, 1981. Atas. São Paulo, SBG. v. 1, p. 148-154.

Pisarevsky, S.A., Biswal, T.K., Wang, X.-C., De Waele, B., Ernst, R., Söderlund, U., Tait, J.A., Ratre, K., Singh, Y.K., Cleve, M., 2013. Palaeomagnetic, geochronological and geochemical study of Mesoproterozoic Lakhna Dykes in the Bastar Craton, India: implications for the Mesoproterozoic supercontinent. Lithos 174, 125–143.

Pouclet, A., Lee, J., Vidal, P., Cousens, B., Bellon, H., 1994. Cretaceous to Cenozoic volcanism in South Korea and in the Sea of Japan: magmatic constraints on the opening of the back-arc basin. In: Smellie, J.L. (Ed.), Volcanism Associated with Extension at Consuming Plate Margins. Geological Society Special Publication 81, 169–191.

Prazeres Filho, H.J., 2005. Caracterização geológica e petrogenética do Batólito Granítico Três Córregos (PR-SP): Geoquímica isotópica (Nd-Sr-Pb), idades (ID-TIMS/SHRIMP) e $\delta^{18}O$ em zircão. Doctor of Science Thesis, Geosciences Institute, University of São Paulo, 207p.

Renne, P.R., Swisher, C.C., Deino, A.L., Karner, D.B., Owens, T., Depaolo, D.J., 1998. Intercalibration of Standards, absolute ages and uncertainties in $^{40}Ar/^{39}Ar$ dating. Chemical Geology 145, 117–152.

Reis Neto, J.M., 1994. Faixa Itaiacoca: Registro de uma colisão entre dois blocos continentais no Neoproterozóico. Doctor of Science Thesis. Geosciences Institute, University of São Paulo, 296 p.

Roberts, N.M.W., 2012. Increased loss of continental crust during supercontinent amalgamation. Gondwana Research 21, 994–1000.

Roberts, N.M.W., 2013. The boring billion? e Lid tectonics, continental growth and environmental change associated with the Columbia supercontinent. Geoscience Frontiers 4, 681–691.

Rogers, J.J.W., Santosh, M., 2002. Configuration of Columbia, a Mesoproterozoic supercontinent. Gondwana Research 5, 5–22.

Sadowski, G.R., 1991. A megafalha de Cubatão no Sudeste Brasileiro. Boletim IG-USP, Série Científica 22, 15–28.

Salazar, C.A., Archanjo, C.J., Rodrigues, S.W.R., Hollanda, M.H.B.M., 2013. Age and magnetic fabric of the Três Córregos granite batholith: evidence for Ediacaran transtension in the Ribeira Belt (SE Brazil). International Journal of Earth Sciences 102, 1563–1581.

Sandeman, H.A., Hanmer, S., Tella, S., Armitage, A.A., Davis, W.J., Ryand, J.J., 2006. Petrogenesis of Neoarchaean volcanic rocks of the MacQuoid supracrustal belt: A back-arc setting for the northwestern Hearne subdomain, western Churchill Province, Canada. Precambrian Research 144, 126–139.

Sato, K., Tassinari, C.C.G., Kawashita, K., Petronilho, L., 1995. O método geocronológico Sm-Nd no IG/USP e suas aplicações. Anais da Academia Brasileira de Ciências 67, 315–336.

Sato, K., Siga Jr., O., Nutman, A.P., Basei, M.A.S., McReath, I., Kaulfuss, G.A., 2003. The Atuba Complex, southern South American platform: Archean components and Paleoproterozoic to Neoproterozoic tectonothermal events. Gondwana Research 6, 251–263.

Sato, K., Siga Jr., O., Silva, J.A., McReath, I., Dunyi, L., Iizuka, T., Rino, S., Hirata, T., Sproesser, W., Basei, M.A.S., 2009. In situ isotopic analyses of U and Pb in zircon by remotely operated SHRIMP II, and Hf by LA-ICP-MS: an example of dating and

genetic evolution of zircon by $^{176}Hf/^{177}Hf$ from the Ita Quarry in the Atuba Complex, SE Brazil. Geologia USP–Série Científica 9, 61–69.

Shuto, K., Ishimoto, H., Hirahara, Y., Sato, M., Matsui, K., Fujibayashi, N., Takazawa, E., Yabuki, K., Sekine, M., Kato, M., Rezanov, A.I., 2006. Geochemical secular variation of magma source during Early to Middle Miocene time in the Niigata area, NE Japan: Asthenosphere mantle upwelling during back-arc basin opening. Lithos 86, 1–33.

Siga Jr., O., 1995. Domínios tectônicos do sudeste do Paraná e nordeste de Santa Catarina: geocronologia e evolução crustal. Doctor of Science Thesis. Geosciences Institute, University of São Paulo, 212 pp.

Siga Jr., O., Basei, M.A.S., Passarelli, C.R., Sato, K., Cury, L.F., McReath, I., 2009. Lower and Upper Neoproterozoic magmatic records in Itaiacoca Belt (Paraná-Brazil): zircon ages and lithostratigraphy studies. Gondwana Research 15, 197–208.

Siga Jr., O., Basei, M.A.S., Sato, K., Passarelli, C.R., Nutman, A., McReath, I., Prazeres Filho, H.J., 2011a. Calymmian (1.50 1.45 Ga) magmatic records in Votuverava and Perau sequences, south-southeastern Brazil: Zircon ages and Nd–Sr isotopic geochemistry. Journal of South American Earth Sciences 32, 301–308.

Siga Jr., O., Cury, L.F., McReath, I., Ribeiro, L.M.A.L., Sato, K., Basei, M.A.S., Passarelli, C.R., 2011b. Geology and geochronology of the Betara region in south-southeastern Brazil: evidence for possible Statherian (1.80–1.75 Ga) and Calymmian (1.50–1.45 Ga) extension events. Gondwana Research 19, 260–274.

Silva, L.C., McNaughton, N.J., Armstrong, R., Hartmann, L.A., Fletcher, I.R., 2005. The Neoproterozoic Mantiqueira province and its African connections: a zircon based U–Pb geochronologic subdivision for the Brasiliano/Pan-African systems of orogens. Precambrian Research 136, 203–240.

Silveira, E.M., Söderlund, U., Oliveira, E.P., Ernst, R.E., Menezes Leal, A.B., 2013. First precise U–Pb baddeleyite ages of 1500 Ma mafic dykes from the São Francisco Craton, Brazil, and tectonic implications. Lithos 174, 144–156.

Soares, P.C., 1987. Seqüências tectono-sedimentares e tectônica deformadora no centro-oeste do escudo paranaense. In: III Simpósio Sul-Brasileiro de Geologia, vol. 2. Atas, Curitiba, pp. 743–771.

Steiger, R.H., Jager, E., 1977. Subcommission on geochronology: convention on the use of decay constants in geo- and cosmochronology. Earth and Planetary Science Letters 36, 359–362.

Stein, D.P.; Campanha, G.A. Da C.; Fernandes, L.A. 1986. A Formação Perau na região de Pilar do Sul. In: Congresso Brasileiro de Geologia, 34, Goiânia, 1986. Anais... Goiânia, SBG. v.2, p.919-930.

Stern, R.A. 1998. High-resolution SIMS determination of radiogenic trace-isotope ratios in minerals. In: Cabri, L.J.; D.J. Vaughan, D.J. (eds.) Modern approaches to ore and environmental mineralogy. Ottawa, Mineralogical Association of Canadá. p. 241-267. (Short Course Handbook, 27).

Stipp, M., Stünitz, H., Heilbronner, R., Schmid, S.M., 2002. The eastern Tonale fault zone: a ‘natural laboratory’ for crystal plastic deformation of quartz over a temperature range from 250 to 700 °C. Journal of Structural Geology 24, 1861–1884.

Sun, S.-S, McDonough, W.F., 1989. Chemical and isotopic systematics of oceanic basalt: implications for mantle composition and processes. In: Saunders, A.D., Norry, M.J. (Eds.), Magmatism in the Ocean Basins. Geological Society Special Publication 42, 313–345.

Takahashi, A.T. et al. 1981. Projeto integração e detalhe no Vale do Ribeira, área Ribeirão do Perau. São Paulo. Convênio DNPM/CPRM. (unpublished report)

Tang, H.-F., Liu, C.-Q., Nakai, S., Orihashi, Y., 2007. Geochemistry of eclogites from the Dabie–Sulu terrane, eastern China: new insights into protoliths and trace element behaviour during UHP metamorphism. Lithos 95, 441–457.

Tassinari, C.C.G., Barbour, A.P., Daitx, E.C.; Sato, K. 1990. Aplicação dos isótopos de Pb e Sr na determinação da natureza das fontes das mineralizações de chumbo do Vale do Ribeira - São Paulo e Paraná. In: Congresso Brasileiro de Geologia, 36, Natal, 1990. Anais... Natal, SBG. v. 3, p. 1254-1266.

Teixeira, W., 1982. Projeto Radambrasil. Folhas SG.21 - Assuncion, SG.22 - Curitiba e SG.23 - Iguape. considerações sobre os dados radiométricos: interpretação e evolução geocronológica. Brasília, Ministério das Minas e Energia.

Tohver, E., van der Pluijm, K.M., Mezger, K., Scandolara, J.E., Essene, E.J., 2005. Two stage tectonic history of the SW Amazon craton in the late Mesoproterozoic: identifying a cryptic suture zone. Precambrian Research 137, 35–59.

Torquato, J.R., Kawashita, K., 1994. Geologia Nuclear V – O método Rb/Sr. Revista de Geologia–Universidade Federal do Ceará 7, 91–124.

Tropper, P., Manning, C.E., 2005. Very low solubility of rutile in H_2O at high pressure and temperature, and its implications for Ti mobility in subduction zones. American Mineralogist 90, 502–505.

Vasconcelos, P.M., Onoe, A.T., Kawashita, K., Soares, A.J., Teixeira, W., 2002. $^{40}Ar/^{39}Ar$ geochronology at the Instituto de Geociências, USP: instrumentation, analytical procedures, and calibration. Anais da Academia Brasileira de Ciências 74, 297–342.

Weber, W., Siga Jr., O., Sato, K., Reis Neto, J.M., Basei, M.A.S., Nutman, A.P., 2004. A Formação Água Clara na Região de Araçaiba-SP: Registro U-Pb de uma Bacia Mesoproterozóica. Geologia USP–Série Científica 4, 101–110.

Williams, I.S., 1998. U-Th-Pb geochronology by ion microprobe. Reviews in Economic Geology 7, 1-35.

Winchester, J.A., Floyd, P.A., 1977. Geochemical discrimination of different magma series and their differentiation products using immobile elements. Chemical Geology 20, 325–343.

Wu, C.-Z., Santosh, M., Chen, Y.-J., Samson, I.M., Lei, R.-X., Dong, L.-H., Qu, X., Gu, L.-X., 2014. Geochronology and geochemistry of Early Mesoproterozoicmeta-diabase sills from Quruqtagh in the northeastern Tarim Craton:Implications for breakup of the Columbia supercontinent. Precambrian Research 241, 29–43.

Table captions

Table 1. Major and trace element geochemical data for meta-mafic rocks from the Votuverava Group. Oxides in wt. %, trace elements in ppm and geographical coordinates in decimal degrees (WGS-84 datum), b.d.l. = below detection limit.

Table 2. Major and trace element geochemical data for meta-mafic rocks from the Votuverava Group (compiled from Faleiros et al., 2011b). Oxides in wt. %, trace elements in ppm and geographical coordinates in decimal degrees (WGS-84 datum).

Table 3. Analytical SHRIMP results for a metabasic rock from the Votuverava Group (GI-7C sample; longitude: -48.5061°, latitude: -24.5174°, WGS-84 datum), with ratios corrected for the ^{204}Pb.

Table 4. ^{40}Ar/^{39}Ar hornblende analytical results for the GD-456 sample (longitude: -48.30049°, latitude: -24.589437°, WGS-84 datum), J factors (0.003744 ± 0.000014), system blanks, and ^{40}Ar/^{36}Ar discrimination (1.0016 ± 0.0034) for the UQ-AGES. The uncertainties are given at the 1σ level.

Table 5. Sm/Nd and Rb/Sr analytical results for metabasic rocks of the Votuverava Group.

Figure captions

Fig. 1. (a) Simplified geotectonic map of part of South America emphasizing cratonic areas and mobile belts (relative to the Neoproterozoic). (b) Simplified geological map of the southern and central portions of the Ribeira Belt with the location of Fig. 2. Geological units: Itaiacoca Group (Ic), Água Clara Formation (Ac), Lajeado Group (L), Votuverava Group (V), Betara Formation (B), São Roque Group (Sr), Serra do Itaberaba Group (It), Socorro-Guaxupé Nappe (Sg), Tigre Gneiss (T), Capirú Formation (C), Turvo-Cajati Formation (Tc), Rio das Cobras Formation (Rc), Atuba Complex (At).

Fig. 2. Simplified geological map emphasizing the Votuverava Group and its formations (modified from Campanha, 1991, Faleiros et al., 2012; Faleiros and Pavan 2013). Also shown are the locations of the analyzed samples. The map uses the Universal Transverse Mercator (UTM) projection, zone 22 south, with the WGS-84 horizontal datum.

Fig. 3. Classification and petrogenetic diagrams with geochemical data of Votuverava metabasites. (a) Ti/V versus Nb/Yb plot, (b) AFM diagram after Irvine and Baragar (1971), (c) SiO_2 versus total alkalis plot after Le Bas et al. (1986), (d) Differentiation index (normative quartz + albite + orthoclase) versus Zr plot, (e) Nb/Y versus Zr/TiO_2 plot after Winchester and Floyd (1977), (f) Zr versus TiO_2 plot.

Fig. 4. Rare earth element (a-d) and incompatible element (e-h) spidergrams of the B1 group Votuverava metabasites. The colored field in (e) is the compositional range for all B1 samples. Data for the Betara Formation metabasites after Siga Jr. et al. (2011b). Samples WX.12, WX.23 and WX.27 are basalts from the East Scotia Ridge back-arc

basin (Leat et al., 2000) for comparison. Normatization values from Sun and McDonough (1989) for MORB and Boynton (1984) for chondrite.

Fig. 5. Rare earth element (a-c) and incompatible element (d-f) spidergrams of the B2 group Votuverava metabasites. The colored field in (d-f) is the compositional range for all B2 samples. Samples WX.12 and WX.23 are basalts from the East Scotia Ridge back-arc basin (Leat et al., 2000) for comparison. Normatization values from Sun and McDonough (1989) for MORB and Boynton (1984) for chondrite.

Fig. 6. Rare earth element (a-c) and incompatible element (d-f) spidergrams of the B3 group Votuverava metabasites. The colored field in (d-f) is the compositional range for all B3 samples. Sample WX.23 is a basalt from the East Scotia Ridge back-arc basin (Leat et al., 2000) for comparison. Normatization values from Sun and McDonough (1989) for MORB and Boynton (1984) for chondrite.

Fig. 7. Cathodoluminescence image of the zircons from the GI-7C sample (Votuverava metabasite).

Fig. 8. Tera-Wasserburg $^{206}Pb/^{238}U$ versus $^{207}Pb/^{206}Pb$ diagram with SHRIMP zircon U–Pb data of sample GI-7C (Votuverava metabasite). Errors are depicted at the 1σ level.

Fig. 9. Incremental-heating spectra for an igneous hornblende grain of sample GD-456, a greenschist facies metabasic rock from the Nhunguara Formation (Votuvera Group).

Fig. 10. Plot of initial $^{87}Sr/^{86}Sr(t)$ versus $\varepsilon_{Nd}(t)$ (t=1480 Ma) (a). Data fields and trends: MORB and mantle array (Winter, 2010), back-arc basin basalts (Shuto et al., 2006; Jian et al., 2008, 2009a,b; Fan et al., 2010), island arc and continental arc volcanics (McCulloch et al., 1994; Winter, 2010). (b) Plot of Sm/Nd versus $\varepsilon_{Nd}(t)$. (c) Sm/Nd isochron diagram of Votuverava metabasites with error ellipses stated at the 2σ level. Also shown are the available zircon U-Pb age data. Circles and ellipses are data from this work. Diamonds are data compiled from Siga Jr. et al. (2011a) (white) and Siga Jr. et al. (2011b) (black).

Fig. 11. Plots of La versus LILE (Cs, Rb, Ba, K_2O, Pb, Sr) (a-f) and HFSE (Th, U, Nb, Ta, Sm, Yb) (g-l) contents.

Fig. 12. Petrogenetic and tectonic discriminant diagrams with geochemical data of Votuverava metabasites. (a) Nb/Yb versus TiO_2/Yb plot (after Pearce, 2008), (b) Nb/Yb versus Th/Yb plot (after Pearce, 2008), (c) Th/Nb versus Ce/Nb plot (modified from Sandeman et al., 2006), (d) Ta/Yb versus Th/Yb plot (after Pearce et al., 1982). Data fields: East Scotia Ridge, Bouvet Island and South Atlantic sediments (Leat et al., 2000; Fretzdorff et al., 2002); Sea of Japan (Pouclet et al., 1994); Mariana Arc (Elliot et al., 1997); MORB and OIB (Pearce et al., 1982); Lau Basin (Pearce et al., 1994); Alaioshan Tectonic Zone (Fan et al., 2010).

Sample	GD109A	GD177	GD391B	GD391G	GD537	IP210B	IP532	IP609	IP637A	IP638B	AP126B
Chemical group	B1	B1	B1	B1	B1	B1	B1	B1	B1	B1	B2
Longitude (W)	48.4271	48.3528	48.4263	48.4263	48.4988	48.5079			48.5854	48.5951	48.7815
Latitude (S)	24.6189	24.6171	24.5535	24.5535	24.5013	24.5170			24.6570	24.6602	24.6962
SiO_2	47.55	50.09	46.87	45.36	48.5	49.36	44.83	47.38	47.29	45.61	50.42
Al_2O_3	13.13	14.48	15.94	14.58	13.69	18.56	12.36	12.92	14.45	14.37	14.29
Fe_2O_3	12.6	10.21	8.62	14.82	8.57	6.99	12.70	15.45	9.13	9.16	11.6
MnO	0.196	0.135	0.176	0.243	0.16	0.148	0.24	0.15	0.162	0.151	0.21
MgO	11.42	8.98	9.73	7.92	10.38	8.05	6.04	4.83	10.94	10.98	7.30
CaO	10.45	9.77	15.96	11.52	13.29	10.29	9.61	5.57	15.02	16.67	7.71
Na_2O	1.51	2.73	0.75	1.83	0.93	2.37	2.15	3.20	1.04	0.68	2.86
K_2O	0.11	0.25	0.18	0.23	0.54	1.36	0.04	b.d.l	0.03	0.05	0.08
TiO_2	0.97	0.483	0.37	0.96	0.3	0.33	1.08	1.44	0.44	0.41	1.383
P_2O_5	0.06	0.04	0.03	0.08	0.03	0.05	0.11	0.13	0.03	0.03	0.1
LOI	1.63	2.58	2.29	2.35	2.24	3.12	11.57	7.79	2.44	2.13	3.01
Total	99.63	99.77	100.9	99.9	98.61	100.63	100.71	98.85	100.97	100.24	98.96
Ba	19	37	19	50	99	340	147.0	8.0	14	44	18
Rb	b.d.l.	10.45	14.33	19.20	21.37	59.29	4.43	b.d.l	b.d.l.	b.d.l.	3.10
Sr	154	143	203	374	78	146	251	62	142	153	364
Zr	45.16	23.07	16.01	49.01	17.44	19.09	65.77	85.27	23.24	21.14	80.59
Cs	b.d.l.	0.38	0.39	0.45	b.d.l.	2.08	2.51	b.d.l	0.13	0.20	0.29
Ga	15.80	11.74	15.52	18.30	12.04	13.29	14.75	17.68	13.97	13.01	16.13
Ta	0.17	b.d.l.	b.d.l.	0.17	b.d.l.	b.d.l.	0.18	0.20	b.d.l.	b.d.l.	0.47
Hf	1.23	0.68	0.46	1.31	0.48	0.55	1.72	2.34	0.63	0.58	2.16
Nb	3.16	1.26	0.80	2.95	0.69	0.86	3.09	3.55	1.11	1.12	6.54
Y	13.64	8.31	8.38	14.49	8.46	8.82	22.49	31.04	8.82	8.41	23.43
Th	0.17	0.13	0.11	0.21	0.16	0.21	0.29	0.38	0.10	0.09	0.90
U	0.07	b.d.l.	b.d.l.	0.08	b.d.l.	b.d.l.	0.10	0.13	b.d.l.	b.d.l.	0.23
V	277	201	203	288	197	168	340	432	206	200	368
Co	54.63	46.06	40.81	56.69	33.72	28.08	39.43	43.38	36.78	35.16	35.59
Cr	569.37	321.02	276.93	23.90	60.43	287.26	63.00	46.91	633.37	691.11	272.65
Ni	233.01	158.10	153.75	113.16	90.42	92.42	70.15	60.56	207.98	200.08	127.56
La	2.82	1.11	1.68	3.06	1.11	1.38	2.79	3.83	1.70	1.71	9.29
Ce	6.42	3.02	2.74	7.90	2.70	3.20	7.71	10.53	3.42	3.19	18.87
Nd	5.83	2.53	2.69	6.19	1.97	2.33	6.47	8.87	3.13	2.96	13.59
Sm	1.87	0.86	0.90	1.92	0.65	0.77	2.10	3.01	1.05	1.00	3.68
Eu	0.73	0.38	0.49	0.87	0.31	0.36	0.85	1.17	0.51	0.50	1.57
Gd	2.13	1.17	1.27	2.21	1.01	1.12	2.71	3.71	1.41	1.35	3.82
Tb	0.41	0.21	0.23	0.43	0.20	0.22	0.56	0.77	0.25	0.24	0.73
Dy	2.55	1.41	1.44	2.72	1.38	1.51	3.82	5.23	1.61	1.51	4.41
Ho	0.50	0.30	0.28	0.54	0.30	0.32	0.77	1.10	0.32	0.29	0.83
Er	1.47	0.92	0.82	1.60	0.92	0.99	2.42	3.37	0.89	0.87	2.44
Tm	0.21	0.14	0.11	0.23	0.14	0.15	0.36	0.53	0.13	0.12	0.36
Yb	1.33	0.95	0.73	1.56	0.98	1.00	2.31	3.45	0.84	0.77	2.28
Lu	0.20	0.14	0.10	0.21	0.14	0.14	0.36	0.51	0.11	0.11	0.31
Sc	41	41	47	37	51	39	43	43	46	45	48
Cu	128.70	30.19	29.47	38.50	42.20	39.81	144.81	88.61	58.48	87.64	105.30
Zn	51.71	58.30	56.18	107.69	53.89	32.98	83.23	56.01	61.52	37.12	b.d.l.
Ge	1.47	3.35	1.77	2.04	1.50	1.53	1.45	1.61	1.56	1.43	2.02
As	b.d.l.	b.d.l.	b.d.l.	6.62	b.d.l.	6.27	6.46	b.d.l	11.48	10.94	b.d.l.
Pr	1.09	0.44	0.49	1.16	0.36	0.45	1.20	1.62	0.56	0.57	2.92
Sb	0.51	0.57	3.58	5.73	0.99	1.49	2.81	5.73	b.d.l.	2.94	2.08
Mo	2.72	3.13	2.97	2.66	b.d.l.	b.d.l.	b.d.l	b.d.l	b.d.l.	b.d.l.	b.d.l.
Sn	b.d.l.	b.d.l.	b.d.l.	b.d.l.	b.d.l.	b.d.l.	b.d.l	b.d.l	b.d.l.	b.d.l.	1.39

Sample	F36	GD396D	GD487	GD541	GD522B	IP037B	AP136	GD456	GD486A	IP474	IP606
Chemical group	B2	B2	B2	B2	B2	B2	B3	B3	B3	B3	B3
Longitude (W)	48.8216			48.4786	48.4863	48.5536	48.7573	48.2988	48.3036	48.6759	48.7382
Latitude (S)	24.6985			24.5017	24.5220	24.6419	24.6910	24.5901	24.5889	24.6871	24.7133
SiO_2	53.4	33.82	42.72	49.08	49.31	46.03	49.12	48.41	49.21	49.94	49.46
Al_2O_3	14.1	14.79	11.93	13.76	13.18	14.17	14.37	14.1	14.38	13.67	14.22
Fe_2O_3	13.74	13.03	12.90	12.42	14.95	13.31	11.27	11.03	11.34	14.42	11.53
MnO	0.181	0.29	0.19	0.19	0.173	0.186	0.167	0.157	0.166	0.198	0.158
MgO	5.60	8.87	5.60	6.39	5.86	8.71	6.99	7.08	7.32	6.08	7.28
CaO	7.19	8.25	9.36	11.42	8.83	11.67	11.1	11.89	11.94	9.00	11.93
Na_2O	3.27	3.20	2.49	1.76	1.67	1.92	2.18	2.09	2.12	3.02	2.25
K_2O	0.05	0.21	0.05	0.17	0.22	0.11	0.05	0.34	0.21	0.27	0.18
TiO_2	1.412	1.28	1.94	1.23	1.498	1.18	1.45	1.48	1.57	2.299	1.446
P_2O_5	0.2	0.13	0.16	0.1	0.13	0.1	0.17	0.13	0.16	0.2	0.15
LOI	1.31	15.05	11.47	2.15	3.5	3.14	1.76	1.82	1.7	0.58	1.5
Total	100.44	98.90	98.80	98.67	99.32	100.52	98.63	98.55	100.11	99.68	100.11
Ba	35	87	59	59	54	45	17	83	60	103	33
Rb	b.d.l.	9.22	2.79	4.96	36.67	4.00	b.d.l.	8.45	5.52	5.41	3.80
Sr	301	289	442	167	141	226	340	393	416	310	506
Zr	142.47	86.91	130.68	64.05	86.25	63.87	106.81	100.03	104.68	167.46	97.57
Cs	0.12	1.32	1.17	0.13	1.30	0.81	b.d.l.	0.20	0.28	0.52	0.25
Ga	20.99	20.33	18.88	16.40	18.78	18.37	17.37	19.05	18.01	21.51	18.15
Ta	0.85	0.35	1.10	0.27	0.33	0.24	0.65	0.71	0.71	1.26	0.66
Hf	3.55	2.26	3.50	1.83	2.34	1.65	2.67	2.77	2.68	4.20	2.50
Nb	9.14	5.44	14.16	5.02	5.20	4.11	9.22	9.46	9.97	14.78	9.19
Y	30.22	20.27	21.69	24.85	26.91	18.04	19.37	19.11	19.78	30.39	19.96
Th	1.72	0.36	1.46	0.58	0.83	0.26	0.93	1.00	1.04	1.82	0.91
U	0.33	0.18	0.42	0.15	0.20	0.08	0.24	0.23	0.27	0.44	0.24
V	382	306	386	346	401	321	320	337	336	409	323
Co	36.28	23.97	37.46	33.45	40.18	42.79	32.24	33.39	34.34	40.11	35.16
Cr	-20.00	223.59	72.92	91.61	80.29	248.73	189.39	248.68	237.29	109.00	120.95
Ni	61.54	114.48	91.77	69.84	73.94	166.35	138.15	141.34	125.84	110.29	123.99
La	6.62	4.10	13.70	6.38	6.89	3.78	9.72	10.12	10.17	19.32	10.67
Ce	13.99	10.91	31.72	15.57	13.47	9.95	21.77	23.31	23.59	35.41	20.68
Nd	11.42	8.59	19.10	9.77	11.83	7.77	14.73	15.28	14.63	26.86	15.12
Sm	3.64	2.60	4.58	2.87	3.47	2.41	3.59	3.86	3.74	6.26	3.74
Eu	1.55	0.83	1.71	1.17	1.44	1.02	1.32	1.45	1.40	2.13	1.43
Gd	4.40	3.05	4.52	3.36	3.92	2.76	3.75	3.77	3.69	6.20	3.80
Tb	0.83	0.60	0.78	0.64	0.77	0.53	0.63	0.66	0.64	1.03	0.64
Dy	5.28	3.83	4.51	4.17	4.96	3.24	3.77	3.96	3.77	5.94	3.78
Ho	1.06	0.75	0.85	0.85	0.99	0.64	0.69	0.74	0.71	1.08	0.71
Er	3.06	2.21	2.36	2.57	3.02	1.86	1.99	2.12	2.04	3.08	2.00
Tm	0.45	0.33	0.33	0.38	0.45	0.27	0.28	0.31	0.29	0.44	0.28
Yb	2.73	2.06	2.03	2.33	2.84	1.65	1.67	1.91	1.80	2.70	1.76
Lu	0.38	0.30	0.30	0.34	0.40	0.24	0.24	0.26	0.26	0.37	0.24
Sc	38	41	32	42	50	42	36	36	36	36	36
Cu	129.02	73.80	91.37	33.97	139.07	94.63	73.23	100.40	109.37	142.44	84.08
Zn	66.68	138.31	97.87	b.d.l.	65.36	81.47	60.63	63.90	38.56	113.27	63.23
Ge	1.59	1.79	1.40	1.35	1.55	1.88	1.50	1.52	1.49	1.94	1.52
As	b.d.l.	33.95	b.d.l	b.d.l.	b.d.l.	10.95	b.d.l.	b.d.l.	12.34	26.75	b.d.l.
Pr	2.25	1.62	4.17	2.03	2.52	1.47	3.04	3.16	3.11	5.78	3.19
Sb	0.35	4.93	5.04	0.23	0.41	6.76	2.29	2.41	5.08	1.37	1.70
Mo	b.d.l.	b.d.l	b.d.l	3.34	b.d.l.	4.01	b.d.l.	b.d.l.	b.d.l.	b.d.l.	b.d.l.
Sn	2.87	b.d.l	b.d.l	b.d.l.	1.25	1.23	1.23	b.d.l.	1.04	1.68	1.04

Sample	388C	398	416D	418	477	492	499B	514B	388	390
Chemical group	B1	B1	B1	B1	B1	B1	B1	B1	B2	B2
Longitude (W)	48.8159	48.8187	48.7504	48.7418	48.6654	48.9282	48.9640		48.8109	48.8251
Latitude (S)	24.8496	24.7890	24.8109	24.8073	24.7066	24.7968	24.8199		24.8488	24.8573
SiO_2	51.78	46.51	47.33	44.56	48.10	50.43	49.73	49.74	47.61	43.63
Al_2O_3	13.63	14.37	14.11	15.69	14.01	14.82	14.05	15.37	12.79	12.69
Fe_2O_3	10.02	13.34	11.65	12.91	13.57	8.86	10.17	13.53	15.72	17.72
MnO	0.27	0.21	0.16	0.50	0.20	0.15	0.25	0.42	0.22	0.23
MgO	8.35	7.93	8.04	7.89	7.96	9.60	6.70	7.08	5.99	7.46
CaO	7.90	12.69	11.57	12.84	10.55	10.99	15.64	7.43	9.56	9.11
Na_2O	4.05	0.98	1.96	0.88	1.92	2.68	0.33	4.24	3.00	1.69
K_2O	0.18	0.17	0.15	0.06	0.09	0.11	0.24	0.12	0.12	0.06
TiO_2	1.02	1.09	0.96	1.03	1.07	0.58	0.72	1.00	1.74	3.34
P_2O_5	0.09	0.10	0.08	0.09	0.10	0.04	0.05	0.08	0.15	0.32
LOI	2.50	2.40	3.80	3.40	2.40	1.50	1.90	0.80	2.90	3.50
Total	99.79	99.79	99.81	99.85	99.97	99.76	99.78	99.81	99.80	99.75
Ba	195.7	45.3	45.8	37.3	65.3	106.6	25.4	11.5	60.3	16.2
Rb	4.0	2.4	3.8	1.7	1.3	1.0	4.6	0.8	1.5	4.7
Sr	63.1	40.3	231.2	54.1	161.6	164.0	574.7	144.8	219.5	176.5
Zr	52.7	56.3	48.4	51.6	62.7	25.3	25.2	48.1	80.6	186.2
Sc	46.0	50.0	48.0	47.0	47.0	41.0	38.0	46.0	43.0	36.0
Ga	11.4	15.5	16.1	20.3	15.7	11.8	16.8	18.9	19.5	20.9
Ta	0.2	0.2	0.2	0.2	0.2	0.1	0.1	0.2	0.4	0.8
Hf	1.7	1.9	1.6	1.6	1.9	0.7	0.7	1.4	2.5	5.7
Nb	3.2	3.6	2.9	2.9	4.1	1.5	1.9	3.3	5.7	13.2
Y	22.3	25.4	20.1	22.3	23.6	12.4	14.6	22.4	30.8	44.5
Th	0.2	0.5	0.2	0.2	0.6	0.2	0.4	1.3	0.4	1.6
U	0.1	0.1	0.1	b.d.l.	0.2	b.d.l.	0.1	0.2	0.1	0.3
V	297	346	302	348	344	221	254	358	430	523
Co	43.6	46.9	45.4	49.3	51.0	42.4	31.6	48.7	49.8	63.9
Cr	167.63	143.68	133.42	119.74	61.58	294.21	164.21	17.11	41.05	92.37
Ni	66.6	44.6	51.2	63.7	43.4	27.4	26.4	20.4	39.8	113.9
La	5.4	5.5	3.9	2.6	4.4	1.5	2.5	4.0	6.8	13.7
Ce	9.5	9.7	8.1	8.1	9.5	4.4	6.2	10.7	14.0	34.2
Nd	8.1	8.8	7.0	7.6	7.5	3.4	5.9	7.6	12.6	26.1
Sm	2.57	2.63	2.16	2.13	2.24	1.21	1.66	2.55	3.50	6.53
Eu	0.81	0.91	0.87	0.87	0.86	0.54	0.89	0.85	1.33	2.16
Gd	3.14	3.43	2.94	3.13	3.29	1.67	2.17	3.14	4.52	7.58
Tb	0.63	0.70	0.59	0.62	0.64	0.34	0.43	0.62	0.87	1.41
Dy	3.81	4.35	3.48	3.74	3.81	2.09	2.40	3.52	5.08	7.98
Ho	0.77	0.86	0.71	0.77	0.84	0.43	0.50	0.78	1.01	1.52
Er	2.07	2.51	2.07	2.19	2.30	1.24	1.44	2.34	2.93	4.24
Tm	0.36	0.39	0.32	0.36	0.38	0.21	0.22	0.38	0.48	0.66
Yb	2.01	2.43	1.88	2.01	2.37	1.16	1.38	2.18	2.87	4.01
Lu	0.30	0.37	0.29	0.32	0.38	0.18	0.21	0.33	0.43	0.59
Cu	130.7	165.7	86.1	126.4	150.7	52.2	78.5	186.7	187.7	364.1
Zn	31	23	33	49	46	16	5	47	53	104
As	b.d.l.	b.d.l.	1.70	2.70	4.50	b.d.l.	0.80	b.d.l.	3.70	0.60
Pr	1.67	1.70	1.39	1.35	1.48	0.70	1.08	1.56	2.39	5.11
Mo	0.2	0.4	b.d.l.	0.4	0.2	0.5	0.3	0.3	0.2	0.2
Au	b.d.l.	0.8	b.d.l.	1.4	2.5	b.d.l.	2.0	1.6	1.5	6.3
Pb	0.2	0.1	0.1	0.8	0.3	7.9	18.3	70.2	0.3	0.5
W	0.2	0.2	b.d.l.	0.2	0.2	0.1	5.8	0.6	0.1	0.3

Sample	401	456B	457	457B	495	501B	516	531	480	531C
Chemical group	B2	B2	B2	B2	B2	B2	B2	B2	B3	B3
Longitude (W)	48.8316	48.8860	48.8919	48.8951	48.9382	48.9618	48.9977	48.9023	48.6776	48.908
Latitude (S)	24.7681	24.7879	24.7937	24.7917	24.7625	24.7927	24.8117	24.7058	24.6902	24.708
SiO_2	47.79	49.62	48.63	47.59	46.85	51.24	49.55	45.82	48.94	49.90
Al_2O_3	14.83	13.21	13.59	13.13	14.92	15.41	13.78	13.15	13.87	14.09
Fe_2O_3	12.72	15.39	15.52	15.83	13.41	10.57	15.95	20.31	14.10	14.21
MnO	0.19	0.21	0.20	0.21	0.20	0.16	0.23	0.26	0.20	0.18
MgO	7.85	6.17	6.19	6.63	7.63	6.57	5.75	5.55	6.37	5.80
CaO	10.91	8.60	9.46	10.61	11.55	10.31	8.47	7.86	8.89	8.71
Na_2O	2.77	2.91	2.84	2.55	2.51	3.19	3.09	1.90	3.12	3.15
K_2O	0.17	0.13	0.20	0.19	0.21	0.37	0.16	0.21	0.29	0.18
TiO_2	1.25	2.04	2.07	2.15	1.40	0.97	1.62	3.38	2.64	2.58
P_2O_5	0.12	0.15	0.14	0.16	0.13	0.09	0.14	0.09	0.20	0.19
LOI	1.20	1.40	1.10	0.90	1.00	1.10	1.10	1.30	1.30	0.90
Total	99.80	99.83	99.94	99.95	99.81	99.98	99.84	99.83	99.92	99.89
Ba	36.3	24.4	56.8	55.8	90.4	27.7	37.2	25.1	89.4	19.4
Rb	1.6	2.0	3.5	2.4	2.4	3.6	1.4	3.0	12.2	1.3
Sr	224.1	147.5	187.3	250.2	143.6	162.7	177.7	252.8	329.6	894.9
Zr	71.2	93.0	93.5	95.8	80.3	67.0	87.5	58.1	142.7	134.3
Sc	41.0	41.0	41.0	42.0	41.0	37.0	48.0	55.0	35.0	33.0
Ga	17.7	17.0	18.0	19.1	18.2	17.2	18.4	19.1	20.6	21.5
Ta	0.2	0.4	0.4	0.4	0.2	0.2	0.3	0.2	1.1	0.9
Hf	2.0	2.9	3.2	3.2	2.6	2.2	2.9	1.9	4.3	4.0
Nb	4.5	6.9	7.1	6.7	4.8	4.2	5.4	2.6	16.3	15.3
Y	23.6	29.3	28.2	28.7	24.7	22.9	27.8	29.0	28.2	30.3
Th	0.5	0.8	0.7	0.7	0.4	0.6	1.2	0.4	2.3	1.7
U	0.1	0.1	0.2	0.1	0.1	0.2	0.2	b.d.l.	0.6	0.5
V	309	424	437	429	320	259	377	942	412	383
Co	51.3	51.9	51.6	51.5	51.9	41.2	50.3	59.0	46.9	44.7
Cr	126.58	47.89	47.89	47.89	106.05	13.68	13.68	3.42	51.32	3.42
Ni	25.2	19.7	22.8	15.0	24.3	21.1	12.8	10.2	30.4	20.3
La	6.1	7.3	6.2	7.1	5.1	3.6	4.3	2.9	18.1	14.4
Ce	13.0	20.3	16.6	18.2	13.6	10.5	9.4	5.7	41.4	35.4
Nd	10.9	13.5	14.0	14.9	11.6	8.8	9.2	8.0	26.3	23.9
Sm	3.23	4.03	3.82	4.00	3.28	2.72	3.06	2.54	5.54	5.52
Eu	1.14	1.43	1.42	1.39	1.19	0.79	1.15	1.03	1.81	1.94
Gd	3.71	4.75	4.59	4.78	3.83	3.21	4.09	3.72	5.64	5.89
Tb	0.72	0.90	0.88	0.89	0.76	0.68	0.86	0.77	1.01	1.04
Dy	4.24	5.31	4.98	5.35	4.16	3.92	5.07	4.58	5.45	5.65
Ho	0.83	1.03	1.01	1.01	0.88	0.76	1.01	1.00	0.98	1.06
Er	2.28	2.85	2.89	2.76	2.45	2.25	3.00	2.85	2.67	2.89
Tm	0.35	0.48	0.46	0.48	0.39	0.36	0.48	0.47	0.39	0.45
Yb	2.26	2.60	2.64	2.59	2.29	2.12	2.76	2.84	2.32	2.49
Lu	0.32	0.38	0.40	0.39	0.36	0.33	0.42	0.45	0.33	0.38
Cu	115.8	100.6	203.3	183.3	133.1	217.0	171.8	4.0	199.0	182.9
Zn	20	24	28	27	23	15	30	50	36	27
As	b.d.l.	3.90	b.d.l.	b.d.l.	b.d.l.	b.d.l.	3.80	11.40	10.00	2.00
Pr	2.14	2.62	2.60	2.85	2.17	1.58	1.75	1.37	5.68	5.28
Mo	0.2	0.2	0.1	0.2	0.2	0.3	0.1	0.2	0.4	0.4
Au	0.7	2.7	3.0	4.5	1.2	2.8	4.1	0.7	1.9	3.4
Pb	0.2	0.2	0.1	0.6	0.1	3.5	1.6	1.1	1.8	0.7
W	0.2	0.3	0.3	0.2	0.1	0.9	0.4	0.6	0.8	0.7

Spot	site	U (ppm)	Th/U	Pb* (ppm)	^{204}Pb (ppb)	f206	^{206}Pb/^{238}U	error	^{207}Pb/^{235}U	error	^{207}Pb/^{206}Pb	error	Age (Ma)				Conc. %
													^{206}Pb/^{238}U	error	^{207}Pb/^{206}Pb	error	
1	m,osc/hd,p,fr	533.6	1.03	170	7	0.00098	0.26441	0.00864	3.39721	0.11619	0.09318	0.00064	1512	44	1492	13	101
2	m,hd,p	365.1	2.10	138	4	0.00089	0.25754	0.00837	3.29300	0.11518	0.09274	0.00088	1477	43	1483	18	100
3	m/c,sz,p	197.0	1.22	65	2	0.00088	0.26334	0.00611	3.38119	0.09599	0.09312	0.00127	1507	31	1490	26	101
4	m/c,hd,fr	190.1	1.06	60	0	0.00020	0.26185	0.00538	3.36793	0.08502	0.09328	0.00115	1499	28	1494	24	100
5	c,hb,fr	125.5	0.83	37	0	0.00002	0.25774	0.00664	3.32274	0.09768	0.09350	0.00106	1478	34	1498	22	99
6	c,hd,p/eq	421.6	1.22	135	1	0.00022	0.25817	0.00569	3.30289	0.07688	0.09279	0.00049	1480	29	1484	10	100
7	e,osc,p,fr	150.0	0.75	44	0	0.00018	0.25963	0.00662	3.37101	0.12893	0.09417	0.00240	1488	34	1511	49	98
8	c/m,h,p,fr	190.1	0.65	55	0	0.00011	0.26188	0.00686	3.35709	0.09605	0.09297	0.00081	1499	35	1487	17	101
9	c,h,eq	173.4	0.56	49	0	0.00013	0.25849	0.00720	3.30487	0.10041	0.09273	0.00085	1482	37	1482	17	100
10	e,osc,ov	308.5	1.03	99	4	0.00098	0.26804	0.00677	3.40159	0.09567	0.09204	0.00089	1531	34	1468	18	104
11	c,hd,p	1406.0	1.13	449	0	0.00002	0.26237	0.00784	3.36597	0.10220	0.09305	0.00027	1502	40	1489	6	101
12	c,hd,p	503.7	1.56	172	0	0.00002	0.25570	0.00780	3.27913	0.10248	0.09301	0.00037	1468	40	1488	8	99
13	c,hd,p	214,3	2,01	82	0	0.00002	0,26179	0,00966	3,35546	0,13642	0,09296	0,00121	1499	50	1487	25	101
14	e,osc,fr	344,4	0,95	103	7	0.00151	0,26040	0,00702	3,31344	0,09586	0,09229	0,00071	1492	36	1473	15	101

Legend:
x.y; grain number followed by analysis number
grain habit; p=prism, eq=equant, rd=rounded, fr=fragment
site; e=end or edge, m=middle, r= rim/vergrowth, c=core
Cl image microstructure; osc=oscillatory zoning, h=homogeneous (d=dark or b=bright)
with asterisk: total Pb in ppm,
without asterisk: isotopic ratios corrected for measured ^{204}Pb;
^{207}Pb/^{206}Pb data corrected with 900 Ma model Pb of Cumming and Richards (1975);
all errors are 1s;

Run ID	$^{36}Ar/^{39}Ar$ Error 1σ	$^{37}Ar/^{39}Ar$ Error 1σ	$^{38}Ar/^{39}Ar$ Error 1σ	$^{40}Ar/^{39}Ar$ Error 1σ	$^{40}Ar^{*}/^{39}Ar$ Error 1σ	$\%Ar^{40}*$ Error 1σ	Age Ma Error 1σ	EMV Axial	Ar^{39} Moles	Ar^{40} Moles
01A	0.0351±0.0094	6.13±0.61	0.0034±0.0024	344±16	335±16	97.12±0.84	1467±49	1.533665	1.36E-17	4.67E-15
01B	0.0077±0.0028	18.74±0.41	0.0034±0.00085	253.2±4.6	255.7±4.8	99.68±0.37	1212±17	1.533665	4.57E-17	1.16E-14
01C	0.0038±0.0027	14.49±0.39	0.0074±0.0011	299.9±5.6	303±5.8	100.01±0.32	1368±18	1.533663	4.91E-17	1.47E-14
01D	0.0042±0.0021	13.08±0.37	0.0076±0.0013	305.6±5.9	308.2±6.1	99.93±0.27	1384±19	1.533670	4.39E-17	1.34E-14
01E	0.0061±0.0032	12.43±0.51	0.0066±0.0015	309.5±8.7	311.4±8.9	99.73±0.35	1394±28	1.533656	2.77E-17	8.58E-15
01F	0.0034±0.005	16.6±1.1	0.0043±0.0022	331±14	335±15	100.09±0.48	1467±44	1.533664	1.75E-17	5.80E-15
01G	0.0026±0.0064	18.8±1.3	0.0089±0.0028	341±16	346±17	100.2±0.6	1499±50	1.533672	1.47E-17	5.00E-15
01H	0.025±0.012	23.6±2.5	0.0039±0.0047	360±34	360±35	98.5±1.1	1540±100	1.533677	7.03E-18	2.53E-15
01I	0.0128±0.0061	26.3±1.1	0.0073±0.0018	303±11	306±12	99.43±0.63	1379±36	1.533679	2.12E-17	6.42E-15
02A	0.136±0.048	19.5±4.6	0.0073±0.0095	1930±410	1910±420	97.99±0.61	3790±350	1.533695	3.60E-18	6.94E-15
02B	0.0163±0.0044	20.84±0.64	0.0052±0.0014	308±7.8	309.4±8.1	98.97±0.49	1388±25	1.533693	3.09E-17	9.53E-15
02C	0.0072±0.002	15.61±0.27	0.0074±0.00073	310.6±4	313.1±4.1	99.7±0.26	1400±13	1.533688	8.76E-17	2.72E-14
02D	0.0062±0.0032	15.56±0.44	0.0043±0.00097	269.2±6.4	271.6±6.6	99.77±0.45	1265±22	1.533688	3.87E-17	1.04E-14
02E	0.0076±0.002	13.54±0.34	0.0054±0.0011	309.3±5.9	311±6.1	99.61±0.28	1393±19	1.533690	5.16E-17	1.60E-14
02F	0.0173±0.0056	13.9±0.66	0.0053±0.0018	279±10	277±11	98.56±0.63	1285±35	1.533683	2.18E-17	6.08E-15
02G	0.009±0.0065	20.07±0.89	0.0069±0.0021	318±12	322±13	99.66±0.63	1427±39	1.533684	1.91E-17	6.08E-15
02H	0.0123±0.0038	22.58±0.8	0.0068±0.0017	352±11	356±11	99.47±0.4	1528±32	1.533686	2.68E-17	9.44E-15
02I	0.048±0.012	29.4±2.1	0.002±0.0033	788±50	792±52	98.48±0.52	2486±88	1.533690	1.17E-17	9.19E-15

$^{40}Ar^{*}$ is the total amount of radiogenic ^{40}Ar obtained by substracting the atmospheric ^{40}Ar and ^{40}ArK from the total ^{40}Ar measured from the sample.

Sample	Group	Sm (ppm)	Nd (ppm)	$^{147}Sm/^{144}Nd$	Error	$^{143}Nd/^{144}Nd$	Error	εNd(t)	T_{DM}* (Ma)	Rb (ppm)	Sr (ppm)	Rb^{87}/Sr^{86}	Error	Sr^{87}/Sr^{86}	Error	$Sr^{87}/Sr^{86}(t)$
GD-109A	B1	2.397	7.923	0.1829	0.0006	0.512609	0.000006	2.06	1750	1.00	236.50	0.0122	0.0001	0.70710	0.00008	0.70684
GI-6	B1	0.738	2.090	0.2137	0.0007	0.512809	0.000016	0.10	1891	11.93	93.18	0.3707	0.0029	0.71438	0.00003	0.70645
GI-7C	B1	0.707	2.020	0.2117	0.0007	0.512846	0.000011	1.21	1813	6.83	113.25	0.1746	0.0014	0.71200	0.00008	0.70827
GI-7D	B1	2.112	6.524	0.1958	0.0007	0.512748	0.000009	2.32	1733	0.31	170.66	0.0052	0.0000	0.71048	0.00004	0.71037
IP-638B	B1	0.864	2.516	0.2075	0.0008	0.512857	0.000013	2.22	1740	0.34	143.15	0.0068	0.0001	0.70471	0.00003	0.70456
M-161G	B1	1.342	3.836	0.2115	0.0022	0.512914	0.000010	2.57	1716	11.51	182.15	0.1833	0.0014	0.72971	0.00011	0.72579
GI-8	B1	1.454	3.884	0.2264	0.0008	0.512967	0.000008	0.77	1844	92.6	194.6	1.3800	0.0080	0.72397	0.00001	0.69466
AP-126B	B2	3.317	12.094	0.1658	0.0006	0.512488	0.000008	2.95	1686	1.08	336.50	0.0093	0.0001	0.71466	0.00002	0.71446
F-36	B2	3.294	9.687	0.2056	0.0007	0.51257	0.000011	-3.02	2112	1.47	281.88	0.0151	0.0001	0.71356	0.00002	0.71324
GD-541	B2	2.823	9.237	0.1848	0.0006	0.512658	0.000011	2.65	1708	7.34	146.13	0.1453	0.0011	0.70540	0.00006	0.70229
IP-37B	B2	2.832	9.315	0.1838	0.0006	0.512636	0.000010	2.41	1725	0.77	433.52	0.0052	0.0000	0.70933	0.00001	0.70922
AP-136	B3	3.478	13.409	0.1568	0.0006	0.512431	0.000008	3.55	1643	0.79	306.94	0.0075	0.0001	0.70506	0.00001	0.70490
GD-456	B3	3.380	12.963	0.1577	0.0005	0.512424	0.000010	3.24	1665	6.89	370.39	0.0538	0.0004	0.70551	0.00006	0.70436
GI-14	B3	5.363	21.865	0.1483	0.0005	0.512344	0.000011	3.46	1648	4.98	299.58	0.0481	0.0004	0.70641	0.00002	0.70538

*Calculated by the two-stage evolution

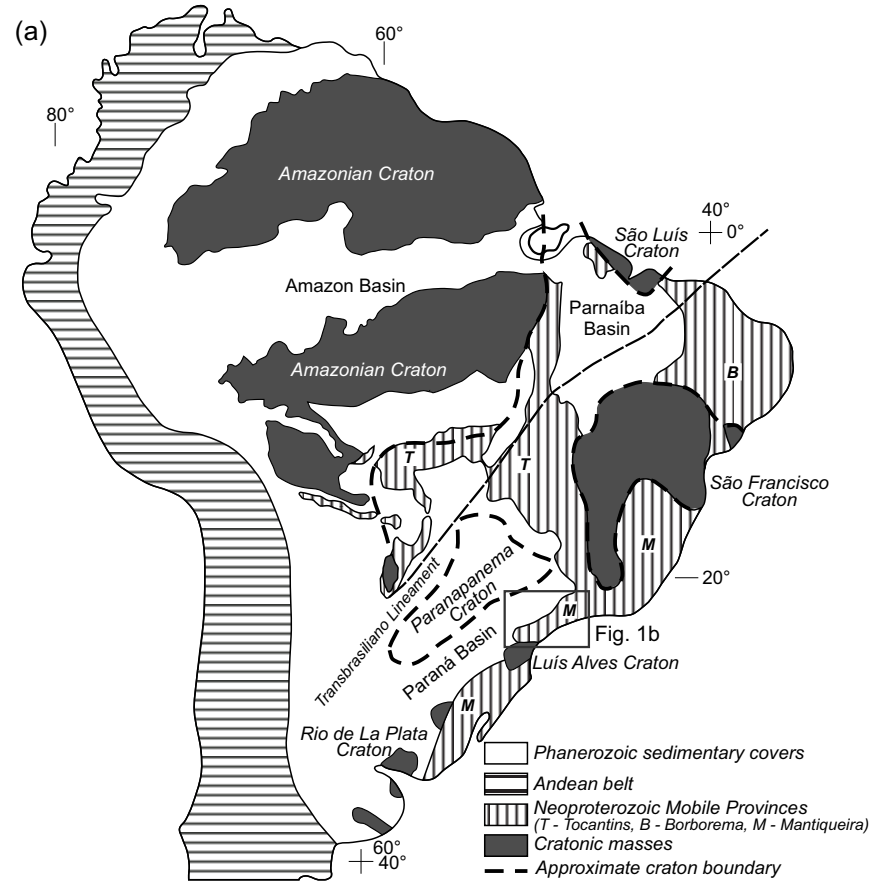
(a)
60°
80°
Amazonian Craton
40°
0°
São Luís Craton
Amazon Basin
Parnaíba Basin
Amazonian Craton
B
T
T
São Francisco Craton
M
20°
Transbrasiliano Lineament
Paranapanema Craton
Paraná Basin
M
Fig. 1b
Luís Alves Craton
M
Rio de La Plata Craton
60°
40°
Phanerozoic sedimentary covers
Andean belt
Neoproterozoic Mobile Provinces
(T - Tocantins, B - Borborema, M - Mantiqueira)
Cratonic masses
Approximate craton boundary

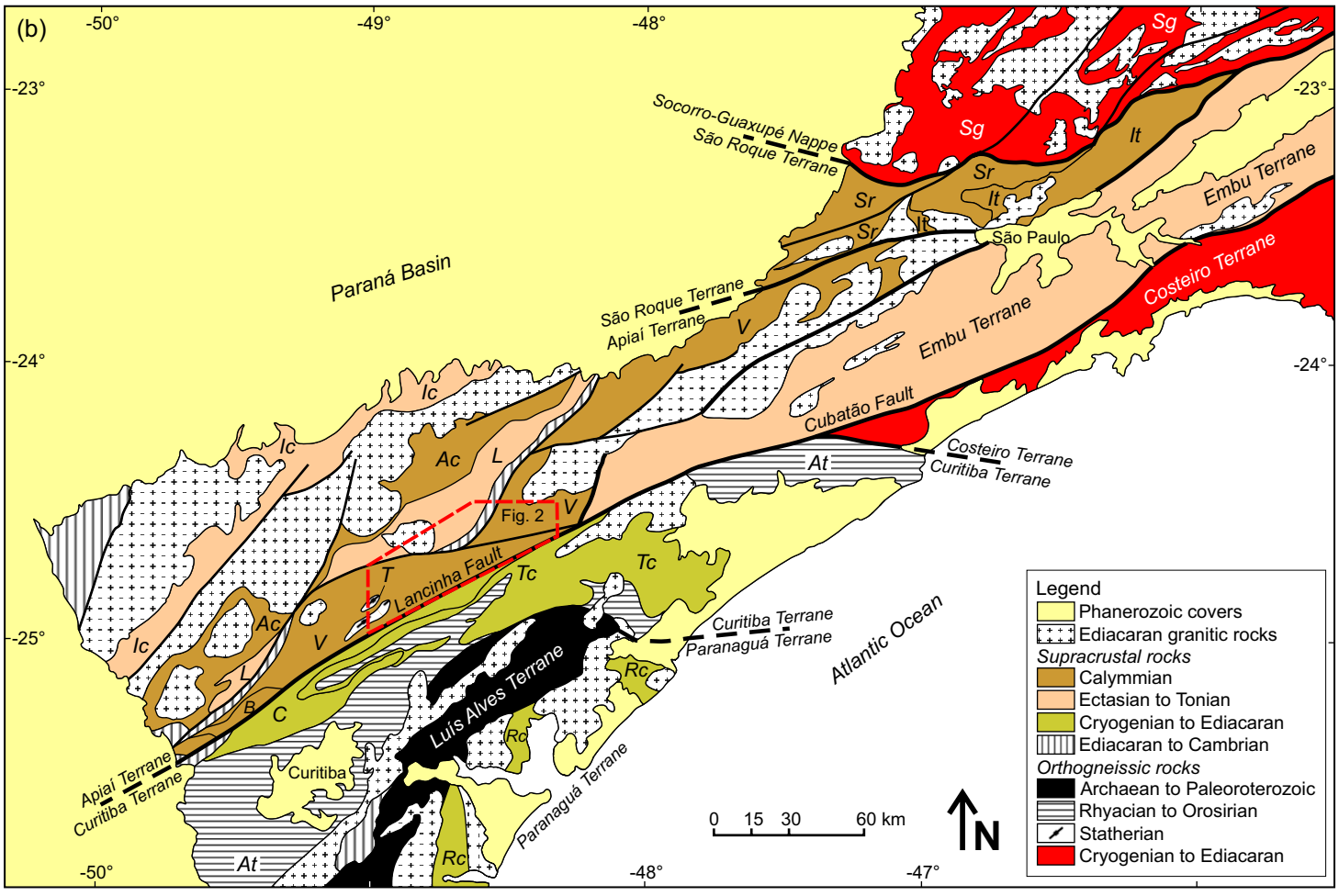
(b)
-50°
-49°
-48°
-23°
-24°
-25°
-47°
Sg
Socorro-Guaxupé Nappe
São Roque Terrane
Sg
It
Sr
Sr
It
Sr
It
São Paulo
Embu Terrane
Costeiro Terrane
Paraná Basin
São Roque Terrane
Apiaí Terrane
V
Embu Terrane
Ic
Ic
Ic
Ac
L
Cubatão Fault
At
Costeiro Terrane
Curitiba Terrane
Fig. 2
V
T
Lancinha Fault
Tc
Tc
Ac
V
Ic
L
B
C
Curitiba Terrane
Paranaguá Terrane
Atlantic Ocean
Rc
Luís Alves Terrane
Rc
Apiaí Terrane
Curitiba Terrane
Curitiba
Paranaguá Terrane
At
Rc
0 15 30 60 km
N
Legend
Phanerozoic covers
Ediacaran granitic rocks
Supracrustal rocks
Calymmian
Ectasian to Tonian
Cryogenian to Ediacaran
Ediacaran to Cambrian
Orthogneissic rocks
Archaean to Paleoroterozoic
Rhyacian to Orosirian
Statherian
Cryogenian to Ediacaran

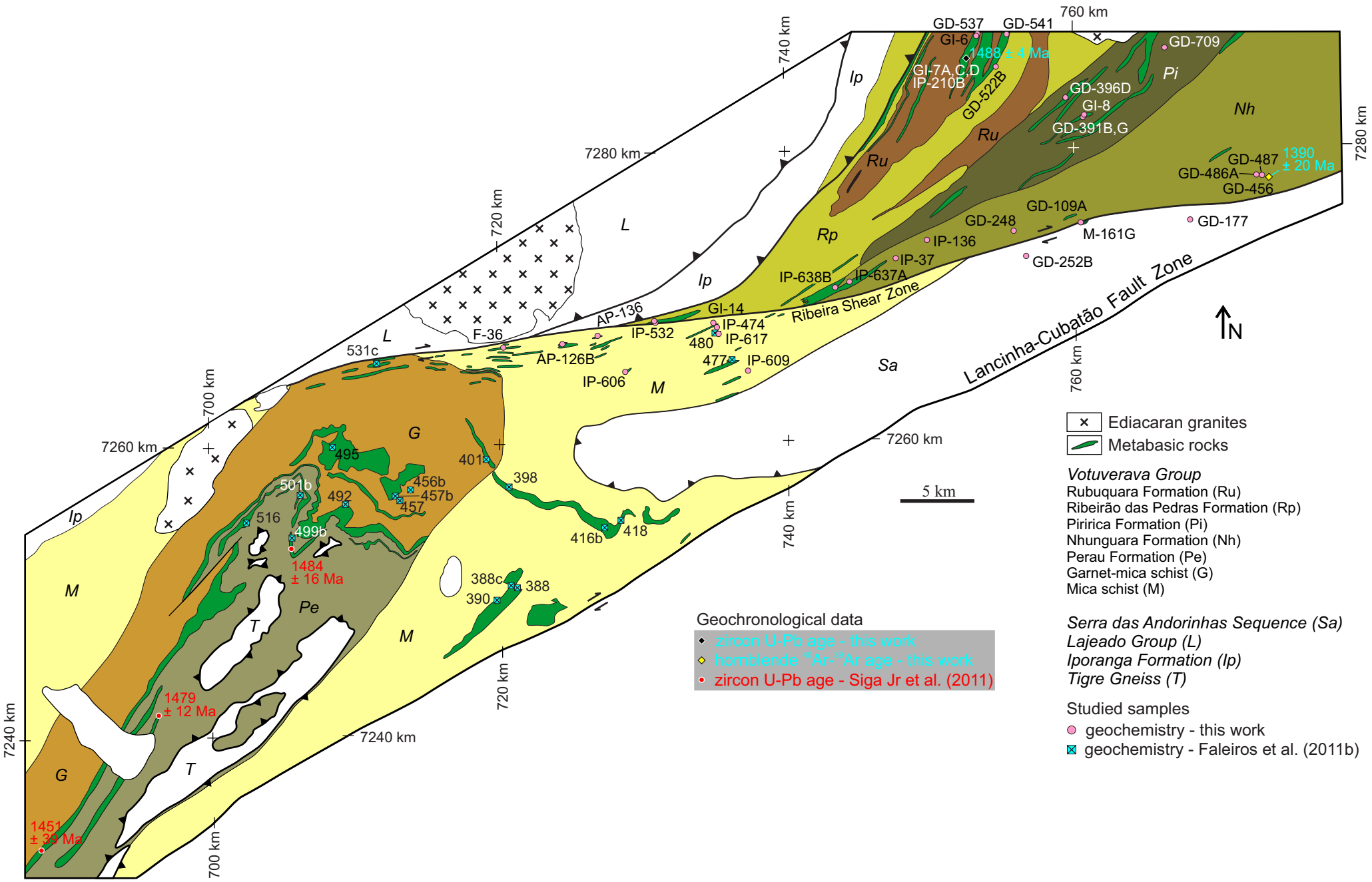
760 km
740 km
720 km
700 km
7280 km
7260 km
7240 km
GD-537
GD-541
GI-6
1488 ± 4 Ma
GI-7A,C,D
IP-210B
GD-522B
GD-709
GD-396D
GI-8
GD-391B,G
GD-487
1390 ± 20 Ma
GD-486A
GD-456
GD-109A
GD-248
M-161G
GD-177
IP-136
IP-37
GD-252B
IP-638B
IP-637A
AP-136
GI-14
IP-532
IP-474
480
IP-617
477
IP-609
AP-126B
IP-606
F-36
531c
Ribeira Shear Zone
Lancinha-Cubatão Fault Zone
N
5 km
Ip
L
Rp
Ru
Pi
Nh
Sa
M
G
T
Pe
495
501b
492
516
499b
456b
457b
457
401
398
416b
418
388c
388
390
1484 ± 16 Ma
1479 ± 12 Ma
1451 ± 39 Ma
Ediacaran granites
Metabasic rocks
Votuverava Group
Rubuquara Formation (Ru)
Ribeirão das Pedras Formation (Rp)
Piririca Formation (Pi)
Nhunguara Formation (Nh)
Perau Formation (Pe)
Garnet-mica schist (G)
Mica schist (M)
Serra das Andorinhas Sequence (Sa)
Lajeado Group (L)
Iporanga Formation (Ip)
Tigre Gneiss (T)
Geochronological data
zircon U-Pb age - this work
hornblende 40Ar-39Ar age - this work
zircon U-Pb age - Siga Jr et al. (2011)
Studied samples
geochemistry - this work
geochemistry - Faleiros et al. (2011b)

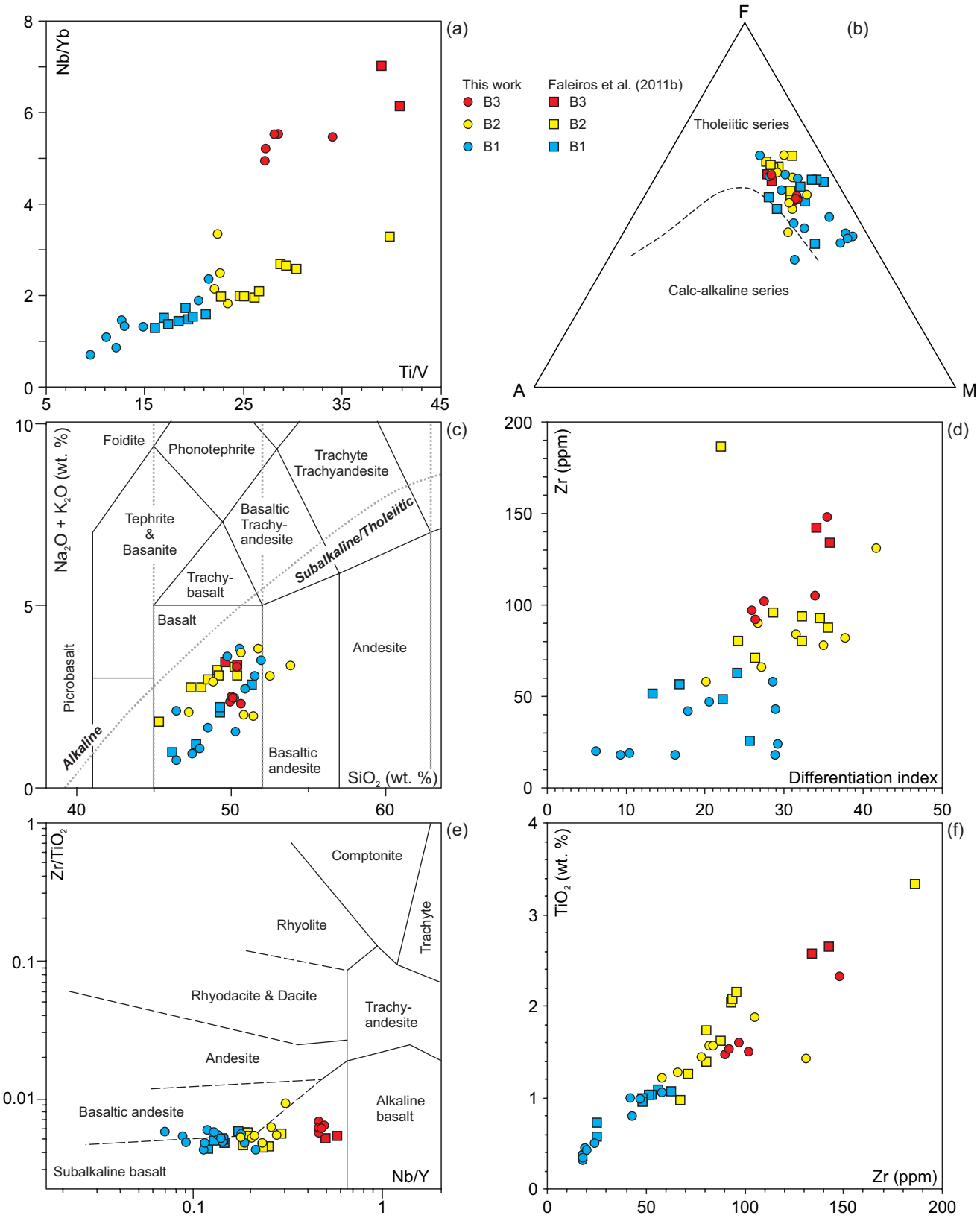
(a)
Nb/Yb
Ti/V
This work
B3
B2
B1
Faleiros et al. (2011b)
B3
B2
B1
(b)
F
A
M
Tholeiitic series
Calc-alkaline series
(c)
Na2O + K2O (wt. %)
SiO2 (wt. %)
Foidite
Phonotephrite
Trachyte
Trachyandesite
Tephrite
&
Basanite
Basaltic
Trachy-
andesite
Subalkaline/Tholeiitic
Trachy-
basalt
Basalt
Andesite
Picrobasalt
Alkaline
Basaltic
andesite
(d)
Zr (ppm)
Differentiation index
(e)
Zr/TiO2
Nb/Y
Comptonite
Rhyolite
Trachyte
Rhyodacite & Dacite
Trachy-
andesite
Andesite
Alkaline
basalt
Basaltic andesite
Subalkaline basalt
(f)
TiO2 (wt. %)
Zr (ppm)

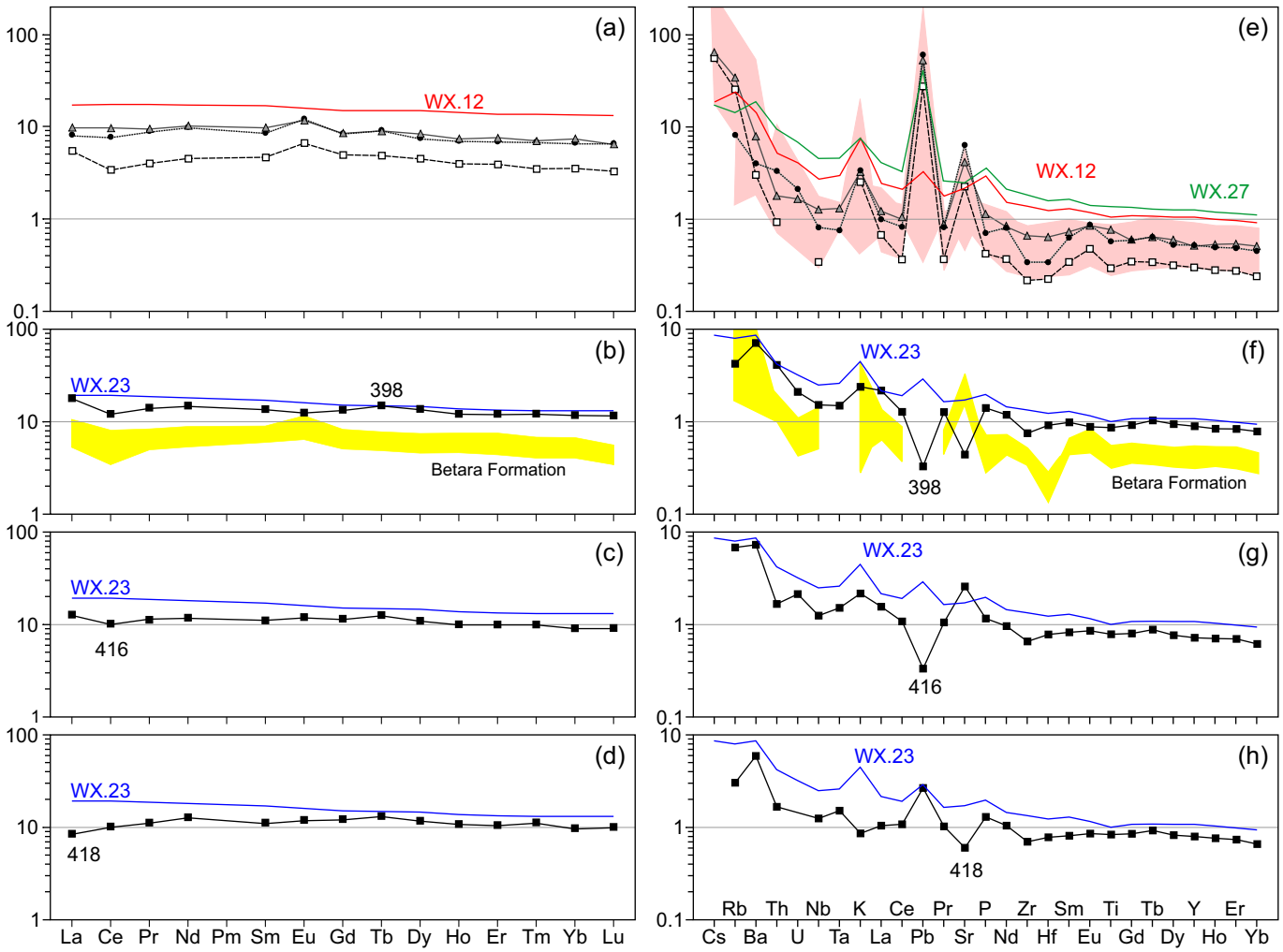
(a)
WX.12
(b)
WX.23
398
Betara Formation
(c)
WX.23
416
(d)
WX.23
418
La Ce Pr Nd Pm Sm Eu Gd Tb Dy Ho Er Tm Yb Lu
(e)
WX.12
WX.27
(f)
WX.23
398
Betara Formation
(g)
WX.23
416
(h)
WX.23
418
Rb Th Nb K Ce Pr P Zr Sm Ti Tb Y Er
Cs Ba U Ta La Pb Sr Nd Hf Eu Gd Dy Ho Yb

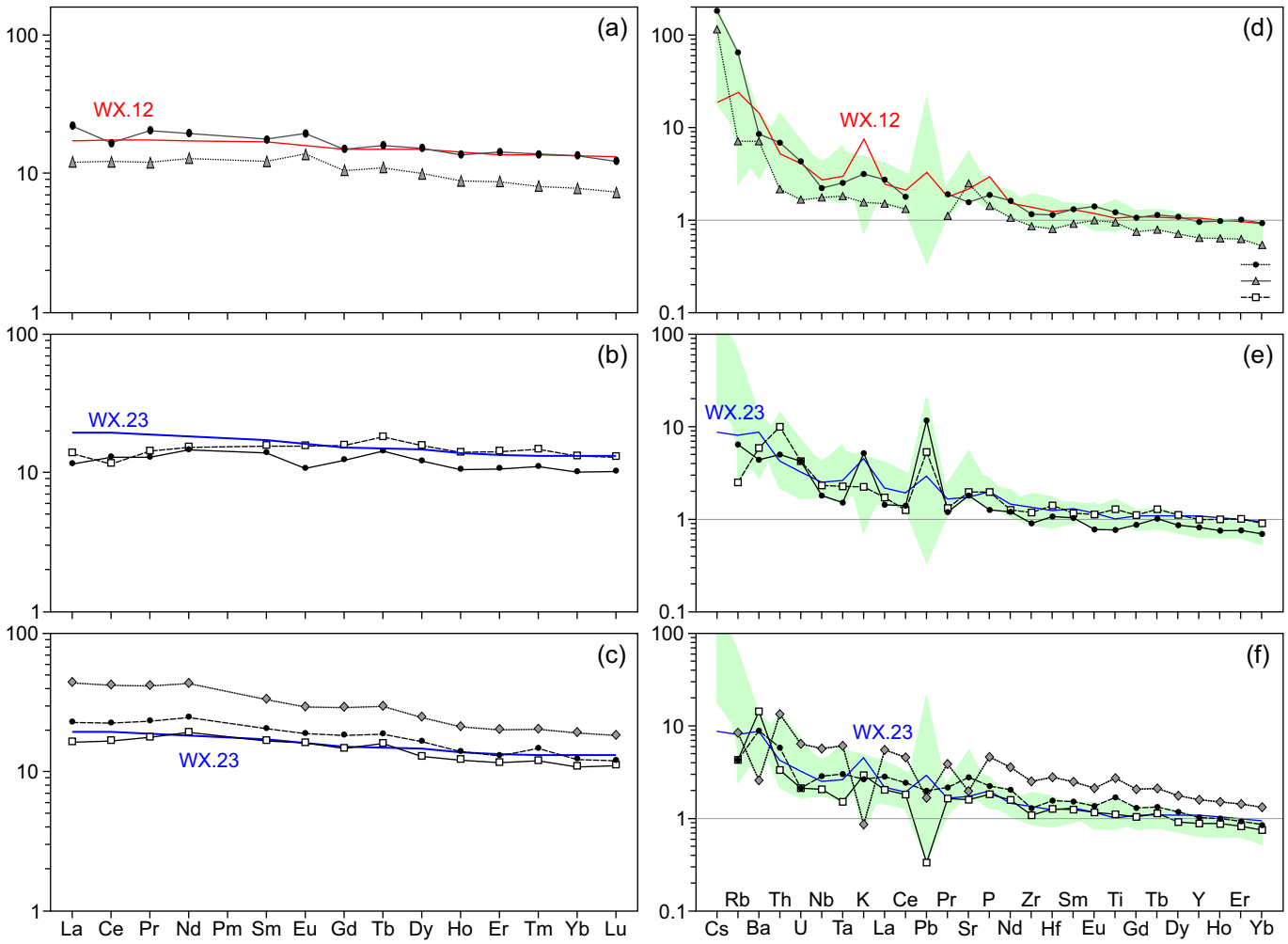
(a)
WX.12
100
10
1
(b)
WX.23
100
10
1
(c)
WX.23
100
10
1
La Ce Pr Nd Pm Sm Eu Gd Tb Dy Ho Er Tm Yb Lu
(d)
WX.12
100
10
1
0.1
(e)
WX.23
100
10
1
0.1
(f)
WX.23
100
10
1
0.1
Cs Ba U Ta La Pb Sr Nd Hf Eu Gd Dy Ho Yb
Rb Th Nb K Ce Pr P Zr Sm Ti Tb Y Er

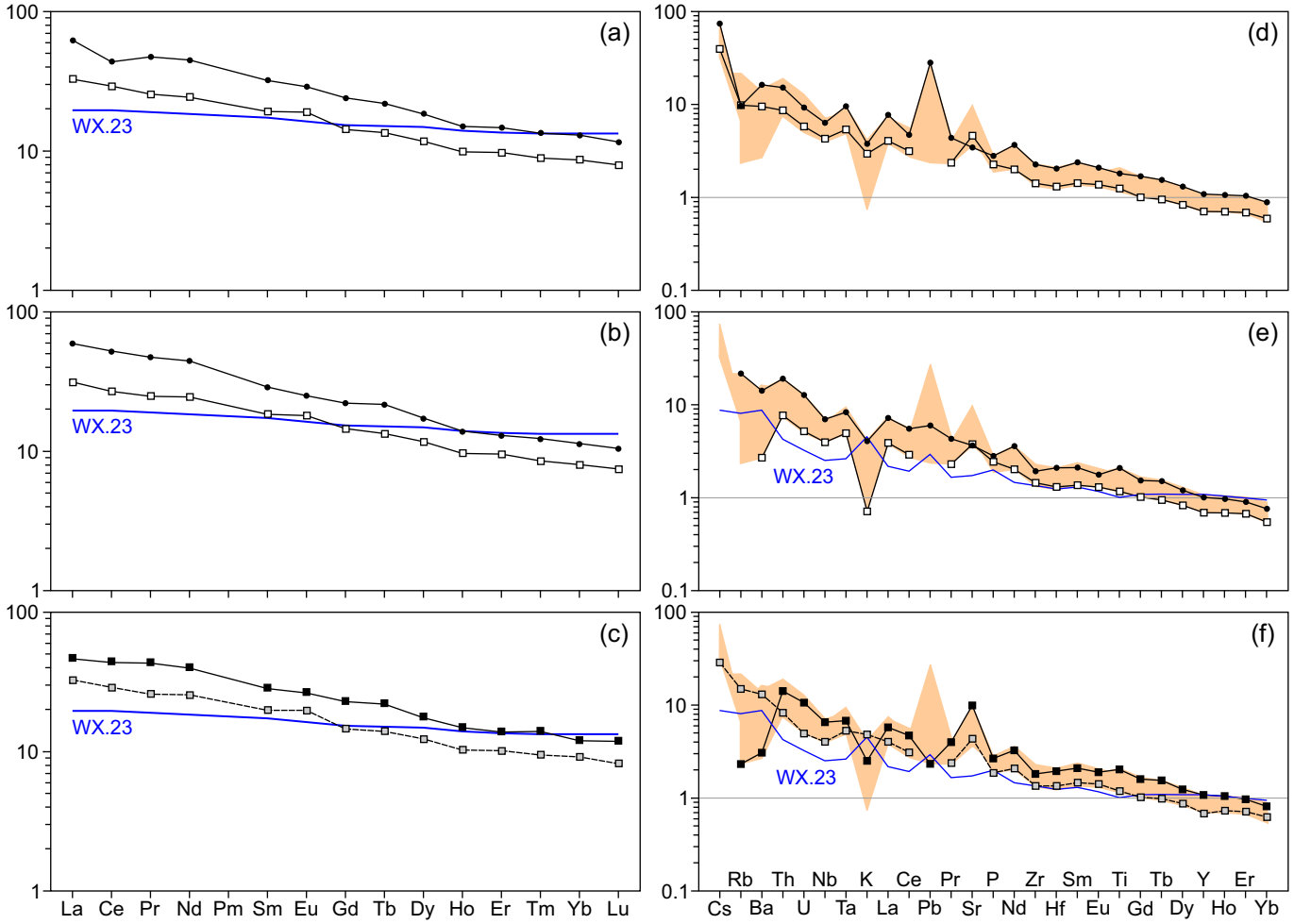
(a)
WX.23
100
10
1
(b)
WX.23
100
10
1
(c)
WX.23
100
10
1
La Ce Pr Nd Pm Sm Eu Gd Tb Dy Ho Er Tm Yb Lu
(d)
100
10
1
0.1
(e)
WX.23
100
10
1
0.1
(f)
WX.23
100
10
1
0.1
Rb Th Nb K Ce Pr P Zr Sm Ti Tb Y Er
Cs Ba U Ta La Pb Sr Nd Hf Eu Gd Dy Ho Yb

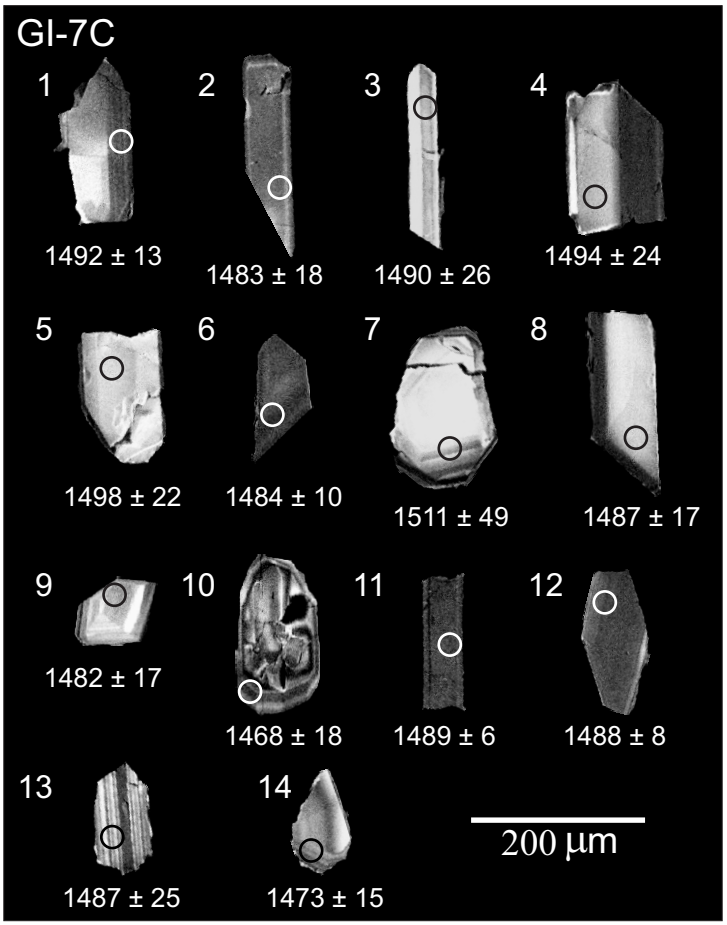
GI-7C
1
1492 ± 13
2
1483 ± 18
3
1490 ± 26
4
1494 ± 24
5
1498 ± 22
6
1484 ± 10
7
1511 ± 49
8
1487 ± 17
9
1482 ± 17
10
1468 ± 18
11
1489 ± 6
12
1488 ± 8
13
1487 ± 25
14
1473 ± 15
200 µm

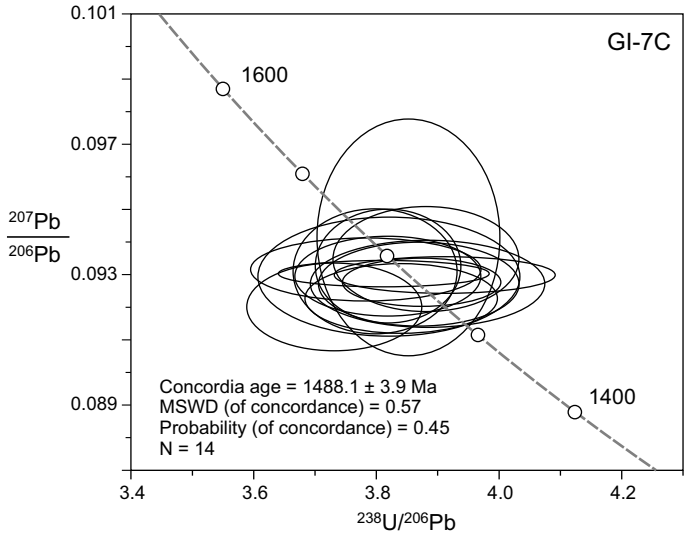
GI-7C
1600
1400
0.101
0.097
0.093
0.089
207Pb/206Pb
3.4
3.6
3.8
4.0
4.2
238U/206Pb
Concordia age = 1488.1 ± 3.9 Ma
MSWD (of concordance) = 0.57
Probability (of concordance) = 0.45
N = 14

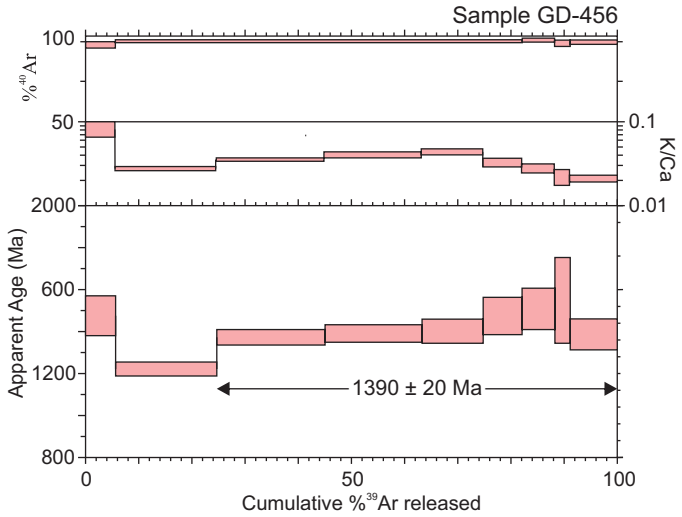
Sample GD-456
100
50
% 40 Ar
0.1
K/Ca
2000
0.01
Apparent Age (Ma)
600
1200
1390 ± 20 Ma
800
0
50
100
Cumulative % 39 Ar released

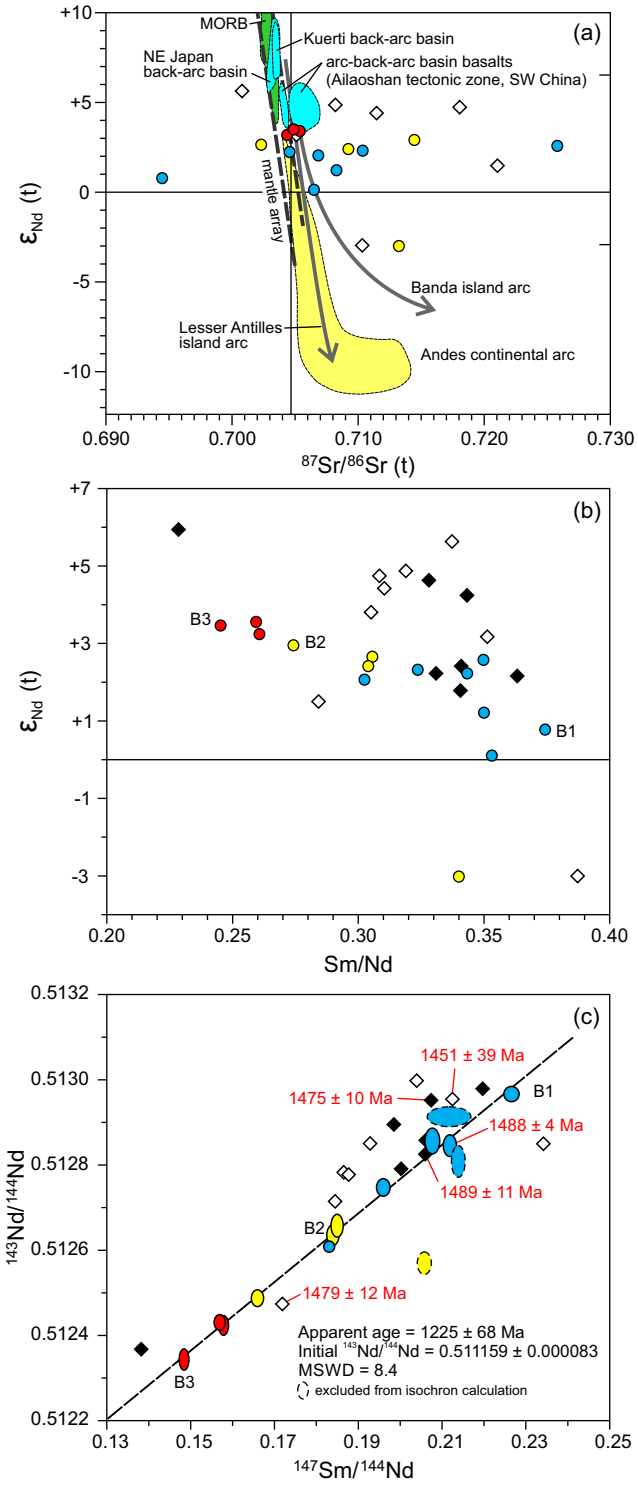
(a)
MORB
Kuerti back-arc basin
NE Japan
back-arc basin
arc-back-arc basin basalts
(Ailaoshan tectonic zone, SW China)
mantle array
Banda island arc
Lesser Antilles
island arc
Andes continental arc
εNd (t)
87Sr/86Sr (t)
(b)
B3
B2
B1
εNd (t)
Sm/Nd
(c)
1451 ± 39 Ma
1475 ± 10 Ma
1488 ± 4 Ma
1489 ± 11 Ma
1479 ± 12 Ma
B1
B2
B3
Apparent age = 1225 ± 68 Ma
Initial 143Nd/144Nd = 0.511159 ± 0.000083
MSWD = 8.4
excluded from isochron calculation
143Nd/144Nd
147Sm/144Nd

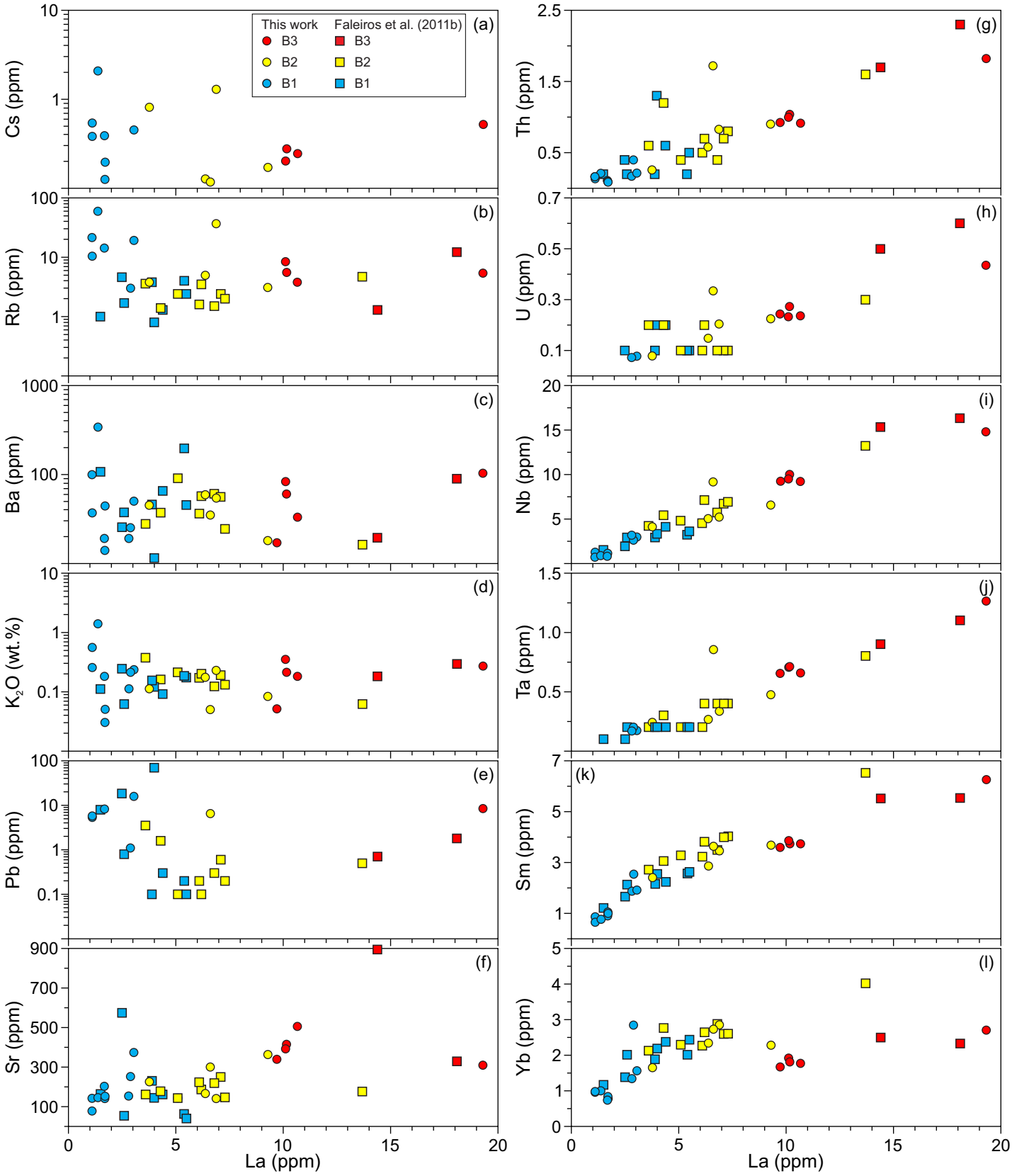
This work
Faleiros et al. (2011b)
B3
B2
B1
B3
B2
B1
(a)
(b)
(c)
(d)
(e)
(f)
(g)
(h)
(i)
(j)
(k)
(l)
Cs (ppm)
Rb (ppm)
Ba (ppm)
K2O (wt.%)
Pb (ppm)
Sr (ppm)
Th (ppm)
U (ppm)
Nb (ppm)
Ta (ppm)
Sm (ppm)
Yb (ppm)
La (ppm)
La (ppm)

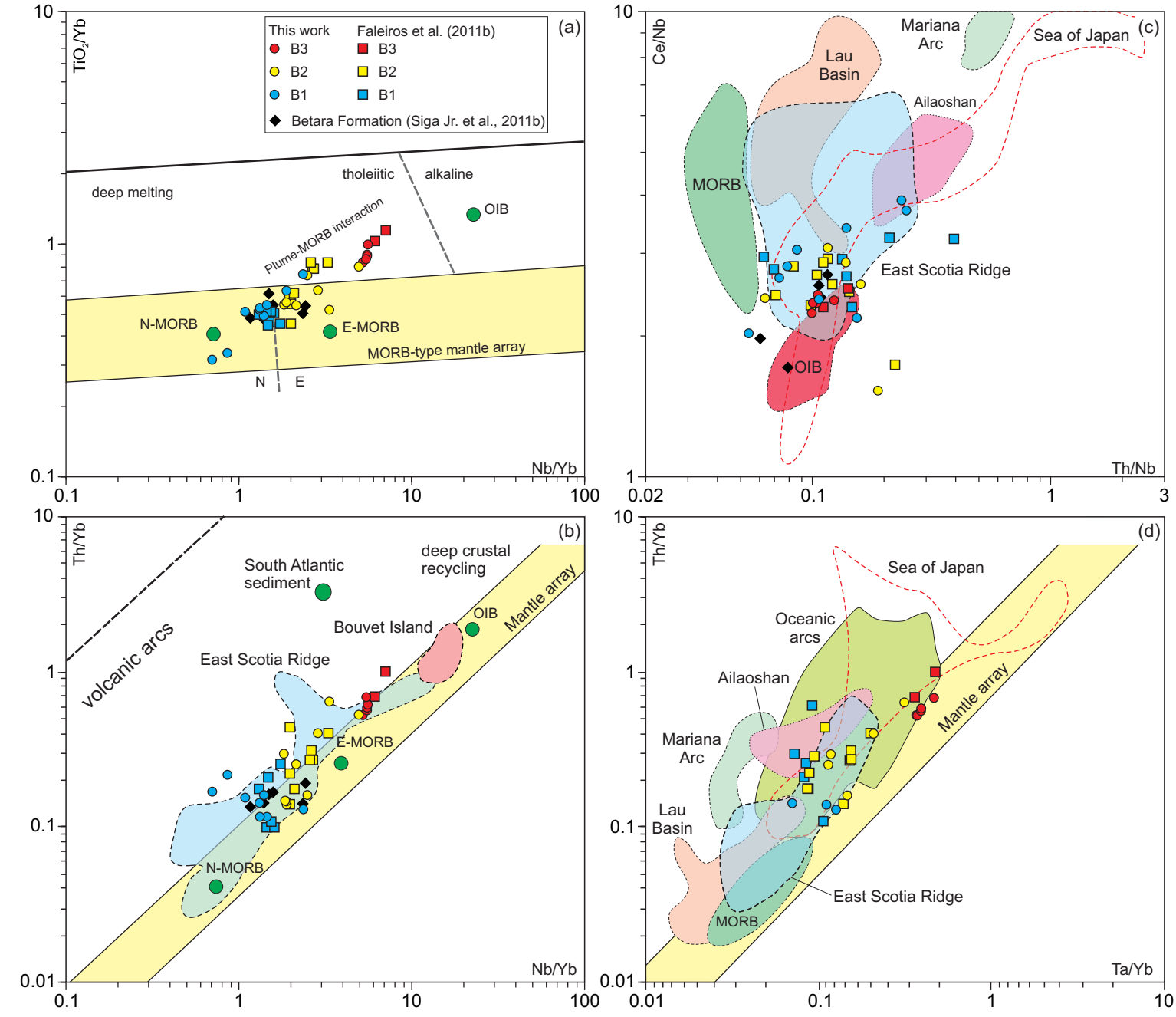
(a)
TiO2/Yb
Nb/Yb
This work
Faleiros et al. (2011b)
B3
B2
B1
B3
B2
B1
Betara Formation (Siga Jr. et al., 2011b)
deep melting
tholeiitic
alkaline
OIB
Plume-MORB interaction
N-MORB
E-MORB
MORB-type mantle array
N
E
(c)
Ce/Nb
Th/Nb
Mariana Arc
Sea of Japan
Lau Basin
Ailaoshan
MORB
East Scotia Ridge
OIB
(b)
Th/Yb
Nb/Yb
South Atlantic sediment
deep crustal recycling
Bouvet Island
OIB
Mantle array
volcanic arcs
East Scotia Ridge
E-MORB
N-MORB
(d)
Th/Yb
Ta/Yb
Sea of Japan
Oceanic arcs
Ailaoshan
Mariana Arc
Mantle array
Lau Basin
East Scotia Ridge
MORB